

# ILVES: Accurate and efficient bond length and angle constraints in molecular dynamics

Lorién López-Villellas,<sup>†</sup> Carl Christian Kjelgaard Mikkelsen,<sup>‡</sup> Juan José Galano-Frutos,<sup>¶</sup> Santiago Marco-Sola,<sup>§,||</sup> Jesús Alastruey-Benedé,<sup>†</sup> Pablo Ibáñez,<sup>†</sup> Miquel Moretó,<sup>§,||</sup> Maria Cristina De Rosa,<sup>¶</sup> and Pablo García-Risueño<sup>\*,⊥</sup>

<sup>†</sup>*Departamento de Informática e Ingeniería de Sistemas, Universidad de Zaragoza, Spain*

<sup>‡</sup>*Department of Computing Science and HPC2N, Umeå, Sweden*

<sup>¶</sup>*Istituto di Scienze e Tecnologie Chimiche “Giulio Natta” (SCITEC), National Research Council (CNR), Italy*

<sup>§</sup>*Barcelona Supercomputing Center, Spain*

<sup>||</sup>*Departament d’Arquitectura de Computadors, Universitat Politècnica de Catalunya, Spain*

<sup>⊥</sup>*Institute for Biocomputation and Physics of Complex Systems, University of Zaragoza, Spain*

E-mail: [lorien.lopez@unizar.es](mailto:lorien.lopez@unizar.es); [risueno@unizar.es](mailto:risueno@unizar.es)

## Abstract

Force field-based molecular dynamics simulations are customarily carried out by constraining internal degrees of freedom. The *de facto* state-of-the-art algorithms for this purpose, SHAKE, LINCS and P-LINCS, converge slowly, impeding high-accuracy calculations and limiting the realism of simulations. Furthermore, LINCS and P-LINCS cannot handle general angular constraints, which restricts increasing the time step. In this paper, we introduce ILVES, a set of parallel algorithms that converge so rapidly that it is now practical to solve bond length and associated angular constraint equations

as accurately as the hardware will allow. We have integrated our work into GROMACS and our analysis demonstrates that, in most cases, our software is superior to the state-of-the-art. We anticipate that ILVES will allow for an increase in the time step, thus accelerating contemporary calculations by a factor of at least 2. This will allow the scientific community to increase the range of phenomena that can therefore be simulated.

## Introduction

Simulation through molecular dynamics (MD)<sup>1,2</sup> has impacted both science and technology<sup>3,4</sup>. It is of special importance in chemistry and medicine, with applications including the design of drugs and catalysts<sup>5-9</sup>, e.g., helping to understand interaction- or mutation-driven biological processes<sup>10-12</sup>. One of the biggest advantages of MD-based approaches is that they provide information on the simulated systems at the atomic level (positions, velocities, forces), which enable the study of phenomena whose analysis in a laboratory is often not feasible or affordable<sup>13,14</sup>. Thanks to recent advancements, particularly in artificial intelligence, the impact of MD is set to grow. For example, the prediction of protein structures through AlphaFold<sup>15</sup> is already boosting massive scale analysis of the behaviour of proteins and their interactions for a variety of relevant areas<sup>16-22</sup>.

In order to be reliable, molecular dynamics must provide an accurate description of existing vibrations of the molecular internal degrees of freedom, such as bond lengths, bond angles, and dihedral angles. It is commonly accepted that simulations must include at least five steps per period for every existing vibration, which sets an upper limit for the time step (i.e., the separation between consecutive simulated times) that can be used. Since the calculation at every time point requires a certain number of arithmetic operations, the size of the time step limits the total real-time that can be simulated using a given computational resource. Therefore, the usual way to carry out MD simulations includes constraining, i.e., freezing, part of the internal degrees of freedom, which is not expected to distort the dynamics

of the simulated system. When only bond lengths are constrained in an MD simulation, the usual size of the time step is 2 fs. Imposing constraints on angles of hydrogen atoms makes it possible to largely increase the time step of the simulation<sup>23,24</sup>. If all bonds and H-angles are constrained, the aforementioned rule of having at least five calculations per vibration period sets approximately 6.4 fs as an upper limit to the time step. Some authors set this limit to 7 fs<sup>25</sup>. Others have indicated that a time step of 4 fs works well (concerning energy conservation) if constraints are imposed on one H-angle and one dihedral angle per hydrogen atom (with the exception of dihedrals of some -C-O-H groups)<sup>26</sup>.

The effect of constraints on the motion of atoms can be modelled through *constraint forces*. For molecules other than water, these forces are customarily calculated using the SHAKE, LINCS and P-LINCS algorithms<sup>27-29</sup>, which have over 43,000 citations at the time of writing this article. These celebrated algorithms, however, present some drawbacks. The constraint solver in the original SHAKE converges slowly and is not considered a good candidate for parallelization. Parallel versions of SHAKE<sup>30,31</sup> have not been widely used and the implementation of SHAKE in GROMACS is sequential (GROMACS is a widely used package for molecular simulation which is thus representative enough to be used as a baseline for our analysis). LINCS is not capable of constraining bond angles in the general case. As a consequence, simulations constraining bond angles are uncommon to date because, in contrast to constraining bond lengths, they do not guarantee clear savings of computing time. In addition, SHAKE, LINCS and P-LINCS are generally applied in a way that results in relatively lower accuracy in satisfying the constraints<sup>32,33</sup>, due to higher accuracy often results in non-negligible additional computing time. In a recent study<sup>33</sup>, we demonstrated that solving constraints inaccurately introduces distortions which can make the simulation unreliable. Insufficient accuracy when solving the constraints is equivalent to applying undesired, spurious and random external forces<sup>33</sup>, which generates a non-negligible drift in the energy of the simulated system that consequently ruins the trustworthiness of simulations in the microcanonical (NVE) ensemble. This has made several studies state that constraint

equations must be solved *down to the limit of computational arithmetic/machine precision*<sup>34,35</sup>. Simulations with a thermostat (NVT, NPT ensembles) also present such undesired energetic drifts, which contribute to making the conserved quantity (also called *conserved energy*) of the thermostat (e.g., Nosé-Hoover, V-rescale) become non-conserved. Due to this, there is no guarantee that the equations of the thermostat are satisfactorily solved, hence there is no guarantee that the simulation corresponds to the sought ensemble, which makes its reliability drop<sup>36,37</sup>. Moreover, the drift introduced by the inaccurate solving of the constraints distorts the time ( $\tau_T$ ) for reaching the sought temperature ( $T$ ). This can be viewed in the V-rescale thermostat<sup>37</sup>, which calculates a rescaling factor for the velocities that, on average, is expected to make the temperature of the system approximately equal to the desired temperature  $T$  after a simulated time  $\tau_T$  (being  $\tau_T$  an input parameter of the simulation). However, due to the inaccurate constraint solving, an additional amount of energy is injected into (or extracted from) the system, which makes the average time for reaching  $T$  deviate from  $\tau_T$  in an unknown manner. In addition, imposing constraints inaccurately systematically misestimate bond lengths and makes them randomly change their values in an irregular manner. Moreover, artifactual regimes arise as periods where the averages of the lengths of the bonds differ from the values set by constraints, which alternate with periods where the bond lengths remain nearly unchanged<sup>33</sup>. In GROMACS, the default SHAKE tolerance (shake-tol, defined as the maximum relative error allowed when solving constraints) is  $10^{-4}$ . There exists no such demanded tolerance for LINCS and P-LINCS, but the average accuracy of these solvers with the default GROMACS parameters is typically similar to SHAKE's. Such default settings lead to the non-negligible distorting effects on energy drifts and bond lengths mentioned above<sup>33</sup>. Other research works have also found non-negligible distorting effects due to inaccurate constraint solving: Ref.<sup>32</sup> stressed that GROMACS' default parameters lead to non-converged results and make temperatures of the simulated system unreliable; others indicate that inaccuracy in constraints can lead to spurious phase transitions<sup>38</sup> and temperature gradients<sup>32</sup>, or the so-called flying ice cube effect<sup>39</sup>.



The array of inconveniences of inaccurate constraint solving can be largely dampened if the constraint forces are calculated with the largest possible accuracy instead of the default value of  $10^{-4}$ . Nevertheless, doing so has been precluded to date due to numerical complexity issues.

## The ILVES algorithms

ILVES is a family of algorithms to impose constraints in the context of MD. They compute discrete approximations of the solution from the same system of differential algebraic equations as the SHAKE algorithm, but they use different methods for solving the constraint equations. In this paper we present two algorithms, ILVES-M (“main”) and ILVES-F (“fast”), that are suitable for general molecules and leverage distributed memory parallelism, shared memory parallelism, and vectorization. Both apply direct solvers (*analytical* solvers, based on Gaussian elimination) to solve the involved linear systems of equations. In a previous article<sup>33</sup>, we introduced ILVES-PC, a proof-of-concept of the application of direct solvers and Newton’s method to calculate constraint forces in biological molecules (peptides and proteins, specifically). In this paper we include results of ILVES-PC for the sake of a more complete analysis of the performance. The original SHAKE algorithm uses the non-linear Gauss-Seidel method to solve the constraint equations, which converges locally and linearly. ILVES-M and ILVES-F have rates of convergence which are far superior to that of SHAKE. ILVES-M and ILVES-F are hybrid methods that rely on a combination of mathematical approximations as well as iterative and direct methods to accomplish their goal. ILVES-M considers the linear systems  $\mathbf{Az} = \mathbf{g}$  that are needed for Newton’s method (where  $\mathbf{z}$  is the vector of unknowns and  $\mathbf{A}$  is the coordinate matrix). If ILVES-M is executed in a single domain, it is a Newton’s method with quadratic convergence. In distributed memory executions, ILVES-M is a quasi-Newton method with linear convergence, as is ILVES-F. In distributed memory executions of ILVES-M, every domain uses a *local* approximation of the matrix-vector

product  $\mathbf{z} = \mathbf{A}^{-1}\mathbf{g}$  instead of solving the full linear system  $\mathbf{Az} = \mathbf{g}$ . Therefore each local approximation is obtained by solving a nonsymmetric linear system using a thread-parallel sparse direct solver based on Gaussian elimination. Since the coordinate matrices in ILVES-M are nearly symmetric, ILVES-F uses fixed symmetric approximations to reduce computations and accelerate the execution.

Detailed information about the mathematical fundamentals of ILVES and its implementation can be found in the Supplementary Materials.

## Results

We have carried out numerous test calculations to gauge the efficiency and reliability of ILVES. Our tests cover different kinds of representative molecules: proteins, DNA, lipids and organic solvents. Information about the procedures used to carry them out, as well as our reliability analysis, can be found in the Supplementary Materials. Below we summarize the outcome about performance, comparing ILVES-M, ILVES-F and ILVES-PC against state-of-the-art constraint solvers. To make a fair comparison possible, we modified P-LINCS to guarantee that constraints are satisfied within a given tolerance, as SHAKE does; we call this solver MP-LINCS.

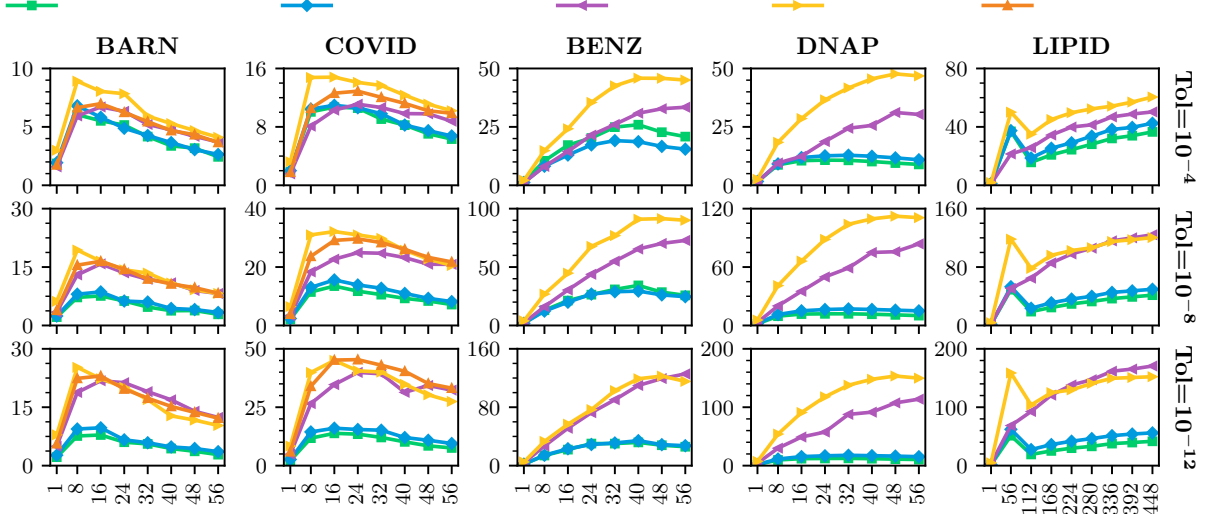
The speed of the constraint solving is closely related to the minimum accuracy demanded. We thus considered three values of the referred tolerance (maximum allowed relative error for every constraint): Tol =  $10^{-4}$  (which is the `-inaccurate`<sup>33</sup> default in GROMACS), Tol =  $10^{-8}$  and Tol =  $10^{-12}$ . The production stage of each of our simulations consisted of 50k steps of size 2 fs.

We have measured the performance of the algorithms for the cases of imposing constraints on either i) hydrogen bonds, ii) all bonds or iii) all bonds together with angles of hydrogen atoms. Constraining only H-bonds is the most usual way to proceed, although it is not as accurate as constraining all bonds (see Supplementary Materials). Constraining the bonds of

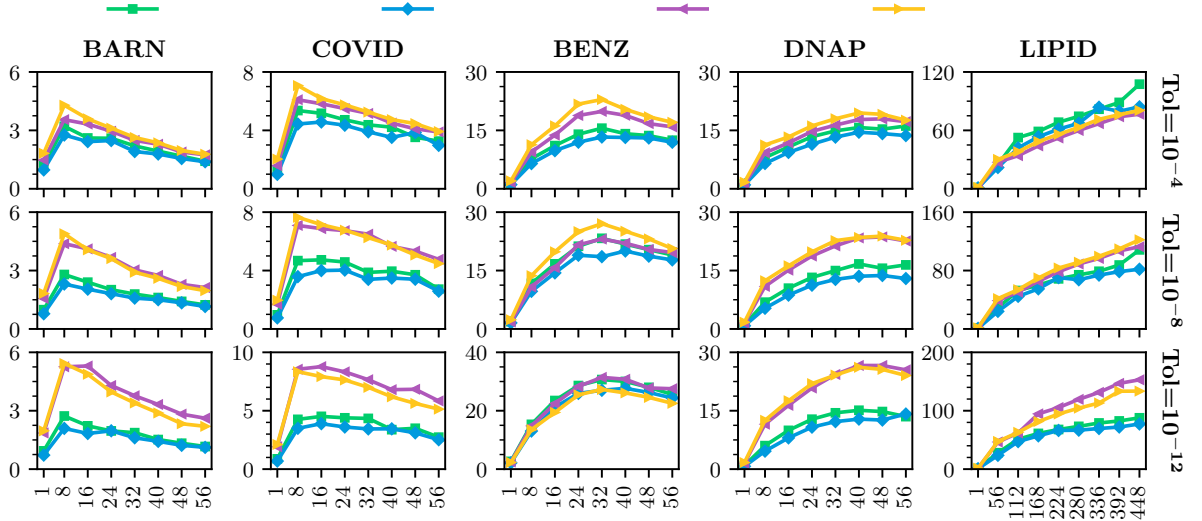
heavy atoms is also a common practice. On the other hand, constraining H-angles has been rather uncommon to date. It is most likely that this is at least partly due to the fact that none of the commonly used constraint algorithms (SHAKE, LINCS and P-LINCS, which are the options offered by GROMACS) can deal with coupled angle constraints satisfactorily: LINCS and P-LINCS often crash while GROMACS’ sequential implementation of SHAKE converges very slowly.

Though solving constraints is sometimes assumed to require a relatively low fraction of the total execution time of simulations, authors inform that it can be as high as 50% or 60%<sup>34,40</sup>. In our simulations constraining all bonds, SHAKE accounts for up to 92% of the total execution time, MP-LINCS up to 42%, and ILVES up to 16%. These percentages depend on the number of cores and are lower in H-bonds simulations, where SHAKE accounts for up to 60%, MP-LINCS up to 6%, and ILVES up to 5%. A detailed figure of the solvers’ relative execution times is provided in the Supplementary Materials.

Fig. 1 presents the *multi-thread* speedup, i.e. the speedup over SHAKE for different numbers of threads and tasks when constraining all bonds and H-bonds. For the barnase (BARN), Covid-19 main protease (COVID), benzene (BENZ) and DNA-protein complex (DNAP), our simulations employed up to 56 threads and 1 task on a single Intel Xeon Platinum 8480+ chip. The larger ( $> 100k$  atoms) lipid bilayer with proteins (LIPID) simulation was executed using up to 8 tasks and 56 threads per task, i.e., up to 4 nodes and 8 chips. In all-bonds simulations (Fig. 1-a), ILVES-M and ILVES-F achieve speedups over (M)P-LINCS across all simulations and tolerances, with a maximum of  $158\times$  over SHAKE and  $14\times$  over MP-LINCS. In H-bonds simulations (Fig. 1-b), MP-LINCS delivers better parallel performance, narrowing the performance gap between the solvers. In these simulations, MP-LINCS only surpasses ILVES-M and ILVES-F in the LIPID simulation at  $\text{Tol} = 10^{-4}$ . On the other hand, ILVES-F delivers better performance than MP-LINCS in the rest of the simulations for a maximum speedup of  $134\times$  over SHAKE and speedups over MP-LINCS ranging from  $0.7\times$  to  $1.8\times$ .



(a) All bonds



(b) H-bonds

Figure 1: Multi-thread speedup over SHAKE of MP-LINCS, ILVES-M, ILVES-F and ILVES-PC<sup>33</sup>. The BARN, COVID, BENZ and DNAP simulations are executed using a single task in a single chip of a computing node. The LIPID simulation is executed using up to 8 tasks (up to 4 nodes and 8 chips). MP-LINCS tested for `lincs-order=4` and `lincs-order=8`. (a) Constraints imposed on all bonds; (b) Constraints imposed on H-bonds.

Despite the fact that tolerance defines the maximum acceptable error, the rapid convergence of the ILVES algorithm often yields errors significantly below this threshold. This results in accuracy gains, providing a compelling reason to choose ILVES over MP-LINCS in simulations where their performance is similar.

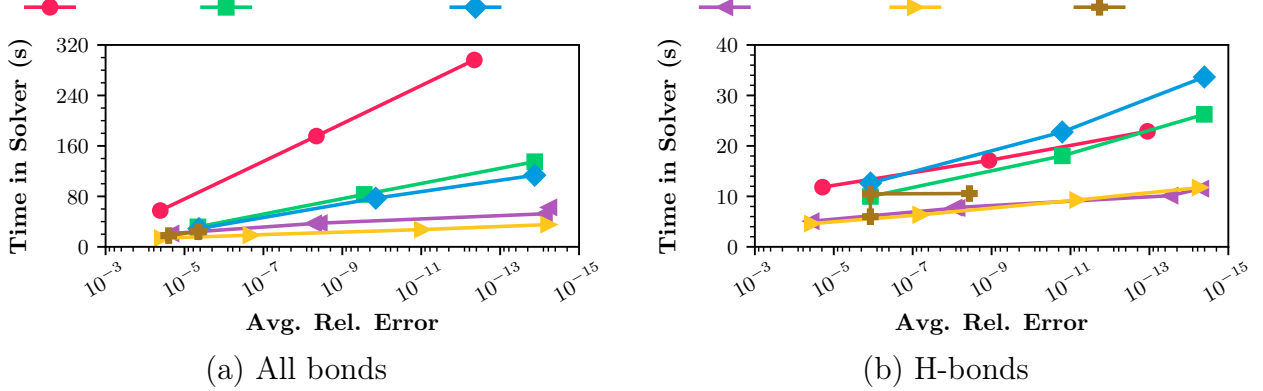
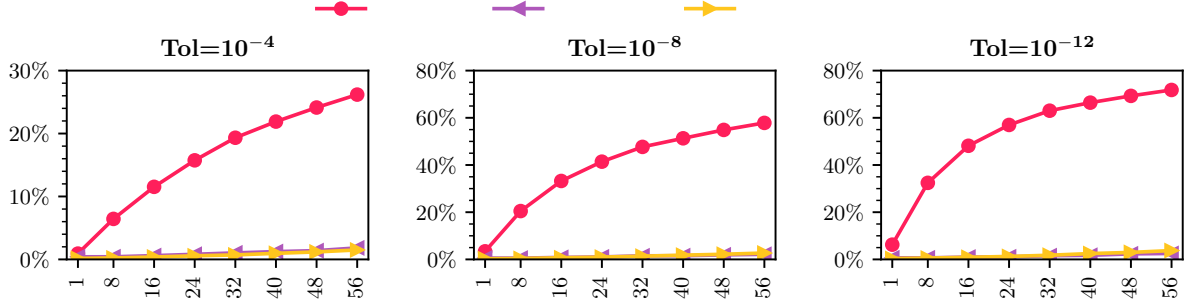


Figure 2: Execution time of the block for solving constraints as a function of the average relative error in satisfying them for different constraint solvers. (a) Constraints imposed on all bonds; (b) Constraints imposed on H-bonds.

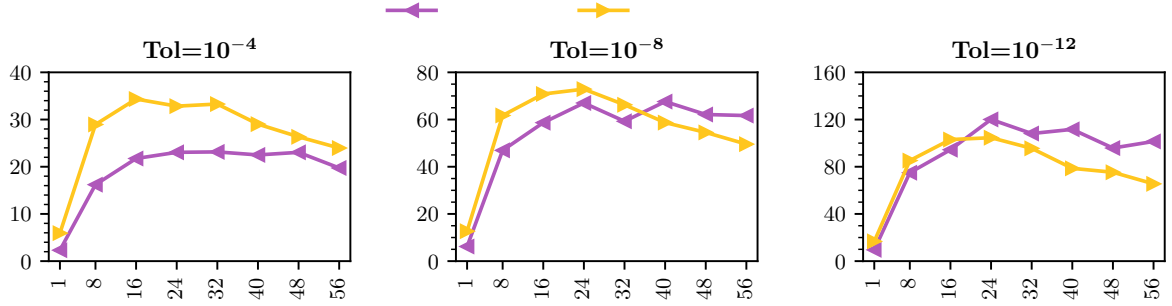
In Fig. 2 we display the execution time required for imposing the constraints as a function of the average relative error, which is defined as the average for  $N_s$  steps and  $n$  constraints that follows:  $\left(\frac{1}{2n \cdot N_s}\right) \cdot \left(\sum_{k=1}^{N_s} \sum_{i=1}^n |\sigma_i^2 - (\mathbf{q}_{a_i}(t_k) - \mathbf{q}_{b_i}(t_k))^2| / \sigma_i^2\right)$ , where  $\mathbf{q}_{a_i}(t_k)$ ,  $\mathbf{q}_{b_i}(t_k)$  are the positions of both atoms joined by the  $i$ th constraint after applying the constraint forces corresponding to the  $k$ th step, and  $\sigma_i$  are the bond length constants. Every point of Fig. 2 corresponds to a run made with different parameters (values of the constraint tolerance for SHAKE; values of the constraint tolerance or number of iterations for ILVES-M and ILVES-F; values of the number of iterations and truncation of the Neumann series —`lincs-iter`, `lincs-order`— for P-LINCS; values of the constraint tolerance and `lincs-order` for MP-LINCS). The results displayed in Fig. 2 correspond to the Covid main protease (4697 constraints) simulated for 50k steps in a single core. If we compare algorithms which ensure that a minimum accuracy is satisfied, like MP-LINCS-O4 and ILVES-F, we observe that, for approximately the same execution time, the latter is far more accurate than the former: for example, for constraints on all bonds, Fig. 2 displays a point for MP-LINCS-O4 whose

execution time is 32 and whose average relative error is  $5 \cdot 10^{-6}$ ; it also displays a point for ILVES-F whose execution time is 27 and whose average relative error is  $9 \cdot 10^{-12}$ . This feature also holds for constraints on hydrogen bonds: examples of points displayed in Fig. 2 are  $(10, 10^{-6})$  for MP-LINCS-O4,  $(9, 7 \cdot 10^{-12})$  for ILVES-F and  $(10, 3 \cdot 10^{-14})$  for ILVES-M. This example indicates that, for similar execution times, the ILVES algorithms are between 500,000 and 30,000,000 times more accurate than P-LINCS algorithms. Fig. 2 indicates that the fast convergence of the ILVES methods makes much more accurate solutions possible requiring very low execution times, making it affordable to solve constraints near the limit of machine precision. We stress that increasing the accuracy of constraint solving is also desirable in simulations made with numerical single precision. In such cases, our tests indicate that the maximum enforceable tolerance is about  $\text{Tol} = 10^{-6}$  instead of the value  $\text{Tol} = 10^{-12}$  which corresponds to double precision;  $\text{Tol} = 10^{-6}$  is much closer to providing converged results of the energy<sup>33</sup> than the default value of  $\text{Tol} = 10^{-4}$ .

Let us now tackle the case of constraining bond angles. Fig. 3 presents a performance analysis using the COVID system for the case of simultaneously constraining all covalent bonds and angles of hydrogen atoms. In this test, the constraints on H-angles are implemented through *triangularization*, i.e. a constraint on the angle between atoms A, B, C with bonds between A, B and between A, C is implemented as an imaginary bond between A, C; this is the method used by GROMACS. As expected, P-LINCS and MP-LINCS cannot correctly impose the constraints. Therefore, we have executed simulations with SHAKE, ILVES-M and ILVES-F. In our tests, SHAKE takes up to 72% of the total execution time of the simulation while ILVES never exceeds 4% (Fig. 3-a). Fig. 3-b shows that ILVES delivers speedups over SHAKE, ranging from  $2\times$  (single-thread, low accuracy) to  $120\times$  (multi-thread, high accuracy). These results indicate that if one increases the time step from, e.g. 2 fs to 4 fs, the gain in execution time would vanish if one used SHAKE. In contrast, ILVES is expected to actually enable such gain, thus allowing either to reduce the computing time by a factor of 2 (for equal total simulated time) or to multiply the simulated time by two (for a given



(a) Percentage of execution time in constraints



(b) Multi-thread speedup over SHAKE

Figure 3: Performance of solvers when constraining H-angles. (a) Percentage of the total execution time taken by SHAKE, ILVES-M, and ILVES-F; (b) Multi-thread speedup of ILVES-M and ILVES-F with respect to SHAKE. Both figures correspond to the COVID system.

amount of execution time).

## Conclusions

In this article we have introduced algorithms based on Newton’s method and on direct linear solvers aimed at imposing constraints on molecular systems. These algorithms present better accuracy and efficiency than the state-of-the-art for constraints on bond lengths. If bond angles are constrained also, the gain in efficiency with respect to existing algorithms is even more remarkable. This is expected to enable researchers to increase the time steps of their molecular dynamics simulations, thus largely reducing the computational burden and enabling the analysis of a wider scope of phenomena.

## Acknowledgement

The authors thank José Alejandro and Edgar Núñez (UAM-Iztapalapa, Mexico) for providing input files of organic solvents.

This work has been partially supported by the Spanish Ministry of Science and Innovation MCIN/AEI/10.13039/501100011033 (contracts PID2022-136454NB-C22, PID2023-146193OB-I00, and PID2023-146511NB-I00), by the Generalitat de Catalunya (contract 2021-SGR-00763 and 2021-SGR-00574), by the Gobierno de Aragón (E45\_20R T58\_23R research groups), and by Lenovo-BSC Contract-Framework Contract (2020). Carl Christian Kjelgaard Mikkelsen is supported by eSENCE, a collaborative e-Science programme funded by the Swedish Research Council within the framework of the strategic research areas designated by the Swedish Government. The funders had no role in study design, data collection and analysis, decision to publish, or preparation of the manuscript.



## Supporting Information Available

- ilves-sup.pdf: Detailed methodology, mathematical background, implementation description, reliability study, extended performance analysis, and an extended study of the importance of accuracy when solving constraints

## References

- (1) Leimkuhler, B.; Reich, S. *Simulating Hamiltonian dynamics*, 1st ed.; Cambridge University Press - Cambridge Monographs on Applied and Computational Mathematics, 2004.
- (2) Karplus, M. Dynamics of folded proteins. *Abstracts of papers of the American Chemical Society* **1978**, *175*, 70.
- (3) Karplus, M.; McCammon, J. A. Molecular dynamics simulations of biomolecules. *Nature Structural Biology* **2002**, *9*, 646–652.
- (4) Hospital, A.; Goñi, J. R.; Orozco, M.; Gelpí, J. L. Molecular dynamics simulations: advances and applications. *Advances and Applications in Bioinformatics and Chemistry* **2015**, *8*, 37–47.
- (5) Shan, X.; Cai, Y.; Zhu, B.; Zhou, L.; Sun, X.; Xu, X.; Yin, Q.; Wang, D.; Li, Y. Rational strategies for improving the efficiency of design and discovery of nanomedicines. *Nature Communications* **2024**, *15*, 9990.
- (6) Andreano, E. et al. SARS-CoV-2 escape a highly neutralizing COVID-19 convalescent plasma. *Proceedings of the National Academy of Sciences* **2021**, *118*.
- (7) Bhardwaj, V. K.; Singh, R.; Sharma, J.; Rajendran, V.; Purohit, R.; Kumar, S. Identification of bioactive molecules from tea plant as SARS-CoV-2 main protease inhibitors. *Journal of Biomolecular Structure and Dynamics* **2021**, *39*, 3449 – 3458.

- (8) Araki, M.; Ekimoto, T.; Takemura, K.; Matsumoto, S.; Tamura, Y.; Kokubo, H.; Bekker, G.-J.; Yamane, T.; Isaka, Y.; Sagae, Y.; others Molecular dynamics unveils multiple-site binding of inhibitors with reduced activity on the surface of dihydrofolate reductase. *Journal of the American Chemical Society* **2024**, *146*, 28685–28695.
- (9) Qiu, X.; Chao, K.; Song, S.; Wang, Y.-Q.; Chen, Y.-A.; Rouse, S. L.; Yen, H.-Y.; Robinson, C. V. Coupling and Activation of the  $\beta$ 1 Adrenergic Receptor-The Role of the Third Intracellular Loop. *Journal of the American Chemical Society* **2024**, *146*, 28527–28537.
- (10) Galano-Frutos, J. J.; García-Cebollada, H.; Sancho, J. Molecular dynamics simulations for genetic interpretation in protein coding regions: where we are, where to go and when. *Briefings in Bioinformatics* **2019**, *22*, 3–19.
- (11) Hollingsworth, S. A.; Dror, R. O. Molecular Dynamics Simulation for All. *Neuron* **2018**, *99*, 1129–1143.
- (12) Kim, C. N.; Shin, D.; Wang, A.; Nowakowski, T. J. Spatiotemporal molecular dynamics of the developing human thalamus. *Science* **2023**, *382*, eadf9941.
- (13) Alonso, J. L.; Chass, G. A.; Csizmadia, I. G.; Echenique, P.; Tarancón, A. In *Meeting on Fundamental Physics ‘Alberto Galindo’*; Alvarez-Estrada, R. F., others, Eds.; Aula Documental: Madrid, 2004.
- (14) Galano-Frutos, J. J.; Sancho, J. Energy, water, and protein folding: A molecular dynamics-based quantitative inventory of molecular interactions and forces that make proteins stable. *Protein Science* **2024**, *33*, e4905.
- (15) Jumper, J.; Evans, R.; Pritzel, A.; Green, T.; others Highly accurate protein structure prediction with AlphaFold. *Nature* **2021**, *596*, 583–589.

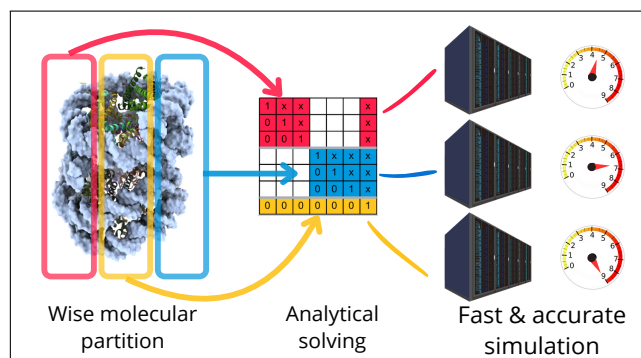
- (16) Li, Y.; Arghittu, S. M.; Dietz, M. S.; Hella, G. J.; Haße, D.; Ferraris, D. M.; Freund, P.; Barth, H.-D.; Iamele, L.; de Jonge, H.; others Single-molecule imaging and molecular dynamics simulations reveal early activation of the MET receptor in cells. *Nature Communications* **2024**, *15*, 9486.
- (17) Lehrer, S.; Rheinstein, P. H. Predicted Configuration and Stability of the ATAD2/SOX10 Complex Using Molecular Dynamics Simulations. *Cancer Diagnosis & Prognosis* **2023**, *3*, 398.
- (18) Zheng, N.; Long, M.; Zhang, Z.; Zan, Q.; Osire, T.; Zhou, H.; Xia, X. Protein-Glutaminase engineering based on isothermal compressibility perturbation for enhanced modification of soy protein isolate. *Journal of Agricultural and Food Chemistry* **2022**, *70*, 13969–13978.
- (19) Osifalujo, E. A.; Rutkowski, B. N.; Satterwhite, L. R.; Betts, P. C.; Nkosi, A. K.; Froese, J. T. Production of novel Rieske dioxygenase metabolites enabled by enzyme engineering. *Catalysis Science & Technology* **2023**, *13*, 3784–3790.
- (20) Meng, B.; Abdullahi, A.; Ferreira, I. A.; Goonawardane, N.; Saito, A.; Kimura, I.; Yamasoba, D.; Gerber, P. P.; Fatihi, S.; Rathore, S.; others Altered TMPRSS2 usage by SARS-CoV-2 Omicron impacts infectivity and fusogenicity. *Nature* **2022**, *603*, 706–714.
- (21) Mosalaganti, S.; Obarska-Kosinska, A.; Siggel, M.; Taniguchi, R.; Turoňová, B.; Zimmerli, C. E.; Buczak, K.; Schmidt, F. H.; Margiotta, E.; Mackmull, M.-T.; others AI-based structure prediction empowers integrative structural analysis of human nuclear pores. *Science* **2022**, *376*, eabm9506.
- (22) Wu, J.; Gu, Z.; Modica, J. A.; Chen, S.; Mrksich, M.; Voth, G. A. Megamolecule Self-Assembly Networks: A Combined Computational and Experimental Design Strategy. *Journal of the American Chemical Society* **2024**, *146*, 30553–30564.

- (23) Stocker, U.; Juchli, D.; van Gunsteren, W. F. Increasing the time step and efficiency of molecular dynamics simulations: optimal solutions for equilibrium simulations or structure refinement of large biomolecules. *Molecular Simulation* **2003**, *29*, 123–138.
- (24) Mazur, A. Hierarchy of Fast Motions in Protein Dynamics. *J. Phys. Chem. B* **1998**, *102*, 473–479.
- (25) Feenstra, K. A.; Hess, B.; Berendsen, H. J. C. Improving efficiency of large time-scale molecular dynamics simulations of hydrogen-rich Systems. *J. Comput. Chem.* **1999**, *20*, 786–798.
- (26) Pechlaner, M.; van Gunsteren, W. F. On the use of intra-molecular distance and angle constraints to lengthen the time step in molecular and stochastic dynamics simulations of proteins. *Proteins: Structure, Function, and Bioinformatics* **2022**, *90*, 543–559.
- (27) Ryckaert, J. P.; Ciccotti, G.; Berendsen, H. J. C. Numerical integration of the Cartesian equations of motion of a system with constraints: Molecular dynamics of n-alkanes. *J. Comput. Phys.* **1977**, *23*, 327–341.
- (28) Hess, B.; Bekker, H.; Berendsen, H. J. C.; Fraaije, J. G. E. M. LINCS: A Linear constraint solver for molecular simulations. *J. Comput. Chem.* **1997**, *18*, 1463–1472.
- (29) Hess, B. P-LINCS: A parallel linear constraint solver for molecular simulation. *J. Chem. Theory Comput.* **2008**, *4*, 116–122.
- (30) Weinbach, Y.; Elber, R. Revisiting and parallelizing SHAKE. *J. Comput. Phys.* **2005**, *209*, 193–206.
- (31) Elber, R.; Ruymgaart, A.; Hess, B. SHAKE parallelization. *Eur. Phys. J. Spec. Top.* **2011**, *200*, 211–223.

- (32) Thallmair, S.; Javanainen, M.; Fábíán, B.; Martínez-Seara, H.; Marrink, S. J. Nonconverged constraints cause artificial temperature gradients in lipid bilayer simulations. *J. Phys. Chem. B* **2021**, *125*, 9537–9546.
- (33) López-Villellas, L.; Mikkelsen, C.; Galano, J.; Marco-Sola, S.; Alastruey, J.; Ibáñez Marín, P.; Moretó, M.; Sancho, J.; García-Risueño, P. Accurate and efficient constrained molecular dynamics of polymers using Newton’s method and special purpose code. *Computer Physics Communications* **2023**, *288*, 108742.
- (34) Hammonds, K.; Heyes, D. Shadow Hamiltonian in classical NVE molecular dynamics simulations: A path to long time stability. *J. Chem. Phys.* **2020**, *152*.
- (35) Toxvaerd, S.; Heilmann, O. J.; Ingebrigtsen, T.; Schrøder, T. B.; Dyre, J. C. Time-reversible molecular dynamics algorithms with bond constraints. *The Journal of Chemical Physics* **2009**, *131*.
- (36) Okumura, H.; Itoh, S. G.; Ito, A. M.; Nakamura, H.; Fukushima, T. Manifold correction method for the Nosé–Hoover and Nosé–Poincare Molecular Dynamics simulations. *Journal of the Physical Society of Japan* **2014**, *83*, 024003.
- (37) Bussi, G.; Zykova-Timan, T.; Parrinello, M. Isothermal-isobaric Molecular Dynamics using stochastic velocity rescaling. *J. Chem. Phys.* **2009**, *130*, 074101.
- (38) Chiu, S.-W.; Clark, M.; Subramaniam, S.; Jakobsson, E. Collective motion artifacts arising in long-duration Molecular Dynamics simulations. *J. Comput. Chem.* **2000**, *21*, 121–131.
- (39) Martinez, J. M.; Elmroth, S. K. C.; Kloo, L. Influence of sodium ions on the dynamics and structure of single-stranded DNA oligomers: A molecular dynamics Study. *Journal of the American Chemical Society* **2001**, *123*, 12279–12289.










- (40) Hammonds, K. D.; Ryckaert, J.-P. On the convergence of the SHAKE algorithm. *Comput. Phys. Comm.* **1991**, *62*, 336–351.

## TOC Graphic



# ILVES: Accurate and efficient bond length and angle constraints in molecular dynamics

## Supplementary Material

Lorién López-Villellas <sup>\*,†</sup> Carl Christian Kjelgaard Mikkelsen <sup>‡</sup> Juan José Galano-Frutos <sup>¶</sup> Santiago Marco-Sola <sup>§</sup> Jesús Alastruey-Benedé <sup>||</sup> Pablo Ibáñez <sup>†</sup> Miquel Moretó <sup>§</sup> Maria Cristina De Rosa <sup>¶</sup> and Pablo García-Risueño <sup>\*,⊥</sup>

<sup>†</sup>*Departamento de Informática e Ingeniería de Sistemas, Universidad de Zaragoza, Spain*

<sup>‡</sup>*Department of Computing Science and HPC2N, Umeå, Sweden*

<sup>¶</sup>*Istituto di Scienze e Tecnologie Chimiche “Giulio Natta” (SCITEC) – National Research Council (CNR), Italy*

<sup>§</sup>*Barcelona Supercomputing Center, Spain / Departament d’Arquitectura de Computadors, Universitat Politècnica de Catalunya, Spain*

<sup>||</sup>*Departamento de Informática e Ingeniería de Sistemas / Aragón Institute for Engineering Research (I3A), Universidad de Zaragoza, Zaragoza, Spain*

<sup>⊥</sup>*Institute for Biocomputation and Physics of Complex Systems, University of Zaragoza, Spain*

E-mail: [lorien.lopez@unizar.es](mailto:lorien.lopez@unizar.es); [risueno@unizar.es](mailto:risueno@unizar.es)



# Materials and Methods

## Theoretical background

In this section, we provide the mathematical foundation for constrained MD. We first summarise the nomenclature used in the equations. Bold lowercase letters (e.g.  $\mathbf{x}$ ) correspond to (column) vectors and bold uppercase letters (e.g.  $\mathbf{M}$ ) represent matrices. If  $\mathbf{A} = [a_{ij}]$  is any matrix, then  $\mathbf{B} = \mathbf{A}^T = [b_{ij}]$  is the transpose matrix given by  $b_{ij} = a_{ji}$ . The Euclidean norm  $\|\mathbf{x}\|$  of a vector  $\mathbf{x} = (x_1, x_2, \dots, x_n)^T \in \mathbb{R}^n$  is the non-negative real number given by  $\|\mathbf{x}\| = \sqrt{\sum_{j=1}^n x_j^2}$ . If the function  $\mathbf{f} = (f_1, f_2, \dots, f_l)^T : \mathbb{R}^n \rightarrow \mathbb{R}^l$  is differentiable, then the Jacobian  $\mathbf{F}(\mathbf{x})$  of  $\mathbf{f}$  at the point  $\mathbf{x} \in \mathbb{R}^n$  is the matrix  $\mathbf{A} = [a_{ij}] \in \mathbb{R}^{l \times n}$  given by

$$a_{ij} := \frac{\partial f_i}{\partial x_j}(\mathbf{x}). \quad (1)$$

In a system of  $s$  atoms, let  $m_i > 0$  denote mass of the  $i$ th atom and let  $\mathbf{m}_i \in \mathbb{R}^3$  and the diagonal mass matrix  $\mathbf{M} \in \mathbb{R}^{3s \times 3s}$  be given by

$$\mathbf{m}_i := (m_i, m_i, m_i)^T, \quad \mathbf{M} := \text{diag}(\mathbf{m}_1^T, \mathbf{m}_2^T, \dots, \mathbf{m}_n^T). \quad (2)$$

In addition, let  $\mathbf{q}_i, \mathbf{v}_i \in \mathbb{R}^3$  denote the position and velocity of the  $i$ th atom, and let  $\mathbf{f}_i \in \mathbb{R}^3$  represent the force acting on it (due to any atom or field). The vectors  $\mathbf{q}, \mathbf{v}, \mathbf{f} \in \mathbb{R}^{3s}$ , which gather all positions, velocities and forces are defined as follows

$$\mathbf{q} := (\mathbf{q}_1^T, \mathbf{q}_2^T, \dots, \mathbf{q}_s^T)^T; \quad \mathbf{v} := (\mathbf{v}_1^T, \mathbf{v}_2^T, \dots, \mathbf{v}_s^T)^T; \quad \mathbf{f} := (\mathbf{f}_1^T, \mathbf{f}_2^T, \dots, \mathbf{f}_s^T)^T. \quad (3)$$

Throughout our text,  $s$  indicates the number of atoms (hence, the total number of Cartesian coordinates for positions is  $3s$ ) and  $n$  indicates the number of imposed constraints.

In the remainder of this section, we present the mathematical details of constrained MD and the ILVES algorithms. First of all, let us note that phenomena of interest for MD

studies span a wide range of time scales. The subset which can be simulated is limited by the time step ( $\Delta t$ ), which is defined as the gap between consecutive simulated times; for force fields-based MD  $\Delta t$  this is typically in the range of femtoseconds (fs). Therefore, setting it to values which are as high as possible (without distorting the dynamics of the simulated system) is a major task. To accomplish this, a widely used method consists of imposing constraints on molecular internal degrees of freedom. Numerous algorithms to perform the corresponding calculations have been proposed, with SHAKE<sup>1</sup> and P-LINCS<sup>2</sup> being the most frequent ones to be applied to molecules other than water.

Molecular dynamics is based on Newton’s second law, which can be written as follows for a system consisting of  $s$  atoms:

$$\dot{\mathbf{q}}(t) = \mathbf{v}(t), \tag{4a}$$

$$\mathbf{M}\dot{\mathbf{v}}(t) = \mathbf{f}(t), \tag{4b}$$

where  $\mathbf{q}, \mathbf{v}, \mathbf{f} \in \mathbb{R}^{3s}$  are the vectors of the positions, velocities and total forces acting on the atoms;  $\mathbf{M}$  is the matrix of (constant) atomic masses and the dot on top indicates time ( $t$ ) derivative.

Internal molecular motions can be classified into three categories: bond lengths, bond angles and dihedral angles (which can be either proper or improper; other motions are e.g. translation, rotation and libration). The internal degrees of freedom have characteristic vibrational frequencies which depend on the involved atoms. For example, the fastest vibrations<sup>3-6</sup> in biological molecules correspond to the stretching of covalent bonds involving a hydrogen atom, stretching of bonds between two non-hydrogen atoms and oscillation of angles comprising at least a hydrogen atom (*H-angles*).

In ref.<sup>6</sup>, the authors carried out an analysis of a protein in vacuum, finding that typical periods of bond stretching motions involving and not involving a hydrogen atom are 10 fs and 20 fs, respectively. The vibrational periods depend on several factors, such as the temperature,

the mass assigned to hydrogen atoms, the scaling factor of force fields and whether or not bond lengths are constrained. For  $T=300\text{K}$ , realistic hydrogen mass, constrained bonds and standard force fields (without arbitrary rescaling of force constants), the vibrational periods of H-angles estimated in Ref.<sup>6</sup> are approximately 20 fs (if the angle comprises 2 hydrogens) and 22 fs (if the angle comprises just one hydrogen). Under these conditions, the next lowest period is that of proper dihedral (*torsion*) angles comprising a hydrogen atom (32 fs)<sup>6</sup>.

As stated in the main article, it is generally assumed that accurate simulations require at least five steps per vibrational period, hence the fastest vibration imposes a limitation on the maximum time step that can be used. If all bonds and H-angles are constrained, this rule sets 6.4 fs as an upper limit to the time step. Research works exist which set this limit to 7 fs<sup>5</sup>. Others have indicated that a time step of 4 fs works well (concerning energy conservation) if constraints are imposed on one H-angle and one dihedral angle per hydrogen atom (with the exception of dihedrals of some -C-O-H groups)<sup>7</sup>; such a way to constrain angles avoids making the molecule excessively rigid, which would happen if one constrained *all* the bond angles a given H atom takes part in (e.g. 6 bond angles in  $\text{CH}_4$ ). Some studies indicate that explicit water introduces fast librational<sup>8</sup> motions (with period  $< 30\text{ fs}$ <sup>6</sup>,  $28\text{ fs}$ <sup>5</sup> or  $40\text{ fs}$ <sup>4</sup>), which sets an upper limit to the time step of  $2\text{ fs}$ <sup>4</sup>. In vacuum simulations, however, constraining bonds and stiff torsional-angles would be feasible, allowing to increase the time step<sup>7</sup>. Also, treating the hydrogens as dummy atoms<sup>5</sup>, or implementing a multistep scheme<sup>4</sup>, where  $2\text{ fs}$  is used for water molecules and a higher time step is used for the rest of biological molecules, which will also enable the use of a longer time step. Other authors<sup>3</sup>, however, indicate that the maximum time step limited by water libration is  $6\text{ fs}$  and that this can even be increased (to e.g.  $10\text{ fs}$ ) by artificially increasing the moments of inertia (i.e. the atomic masses) of the water molecule, which is not expected to distort the physical properties of the simulated system<sup>5</sup>. In ref.<sup>3</sup>, the authors state that the time step in protein MD simulations can be safely raised to  $5\text{ fs}$  if constraints on angles are imposed, and a further increase to  $10\text{ fs}$  is possible if hydroxyl rotations are also constrained. Further research<sup>5</sup> indicates that the

time step can be raised to 7 fs if H-angles are constrained.

If we impose a set of  $n$  constraints on the system (4) then the equations of motion change to a system of differential algebraic equations:

$$\dot{\mathbf{q}}(t) = \mathbf{v}(t), \quad (5a)$$

$$\mathbf{M}\dot{\mathbf{v}}(t) = \mathbf{f}_{ext}(t) - \mathbf{G}(\mathbf{q}(t))^T \boldsymbol{\lambda}(t), \quad (5b)$$

$$\mathbf{g}(\mathbf{q}(t)) = \mathbf{0}. \quad (5c)$$

Here  $\mathbf{g} : \mathbb{R}^{3s} \rightarrow \mathbb{R}^n$  is the constraint function

$$\mathbf{q} \rightarrow (g_1(\mathbf{q}), g_2(\mathbf{q}), \dots, g_n(\mathbf{q})) \quad (6)$$

and  $\mathbf{G}(\mathbf{q}) \in \mathbb{R}^{n \times 3s}$  is the Jacobian of  $\mathbf{g}$  with respect to the vector  $\mathbf{q}$  of atomic coordinates. If the  $i$ th constraint is a bond length constraint between atoms  $a_i$  and  $b_i$ , then

$$g_i(\mathbf{q}) = \frac{1}{2} (\sigma_i^2 - \|\mathbf{q}_{a_i} - \mathbf{q}_{b_i}\|^2). \quad (7)$$

where  $\sigma_i$  is the desired distance between the atoms  $a_i$  and  $b_i$ .

For constant computing resources and constant execution time, the time step limits the total simulated time. Therefore, in order to encompass longer-spanning phenomena one can constrain the fastest internal degrees of freedom, which facilitates a corresponding increase in the time step<sup>7</sup>. To this end, one can impose constraints which set internal degrees of freedom to approximately constant values, i.e. which *freeze* them. This might reduce the physical correctness in some cases<sup>6</sup>, though not necessarily.

The vast majority of computer simulations rely on discrete time steps. Among the standard integrators used to update positions —whether strictly following Newton’s second law or a modification of it— are the Verlet<sup>9</sup> algorithms (e.g., Leapfrog and Velocity Verlet), as well as the Stochastic Dynamics (SD) and Langevin Dynamics algorithms<sup>10</sup>. Verlet integration is

used by the SHAKE algorithm, which solves the system of differential algebraic equations (5) using a pair of staggered uniform time grids with *fixed* time step  $h$ . Its equations can be written as follows<sup>11</sup>:

$$\mathbf{v}_{k+1/2} = \mathbf{v}_{k-1/2} + h\mathbf{M}^{-1}(\mathbf{f}_{ext}(\mathbf{q}_k) - \mathbf{G}(\mathbf{q}_k)^T \boldsymbol{\lambda}_k), \quad (8a)$$

$$\mathbf{q}_{k+1} = \mathbf{q}_k + h\mathbf{v}_{k+1/2}, \quad (8b)$$

$$\mathbf{v}_k = (\mathbf{v}_{k-1/2} + \mathbf{v}_{k+1/2})/2, \quad (8c)$$

$$\mathbf{g}(\mathbf{q}_{k+1}) = \mathbf{0}, \quad (8d)$$

where  $k \in \mathbb{N}$  is the time ( $t$ ) index:  $\mathbf{q}_k \approx \mathbf{q}(t_k)$  and  $\mathbf{v}_{k+\frac{1}{2}} \approx \mathbf{v}(t_{k+\frac{1}{2}})$ ;  $t_k = k \cdot h$  and  $t_{k+\frac{1}{2}} = (k + 1/2)h$ . Equation (8d) is a non-linear equation for the unknown Lagrange multiplier  $\boldsymbol{\lambda}_k$ , namely  $\mathbf{g}(\boldsymbol{\phi}_k(\boldsymbol{\lambda})) = \mathbf{0}$  where  $\boldsymbol{\phi}_k$  is the function given by merging (8a), (8b):

$$\boldsymbol{\phi}_k(\boldsymbol{\lambda}) := \mathbf{q}_k + h \left( \mathbf{v}_{k-\frac{1}{2}} + h\mathbf{M}^{-1}(\mathbf{f}_{ext}(\mathbf{q}_k) - \mathbf{G}(\mathbf{q}_k)^T \boldsymbol{\lambda}) \right). \quad (9)$$

We shall now describe how Newton's method can be applied to constrained MD<sup>12</sup>. Let  $\mathbf{f} : \mathbb{R}^n \rightarrow \mathbb{R}^n$  be a differential function and consider the problem of solving the equations:

$$\mathbf{f}(\mathbf{x}) = \mathbf{0}, \quad (10)$$

with respect to  $\mathbf{x} \in \mathbb{R}^n$ . If the Jacobian  $\mathbf{F}(\mathbf{x})$  of  $\mathbf{f}$  at the point  $\mathbf{x}$  is non-singular, then Newton's method takes the form:

$$\mathbf{F}(\mathbf{x}_l)\mathbf{z}_l = \mathbf{f}(\mathbf{x}_l), \quad (11a)$$

$$\mathbf{x}_{l+1} = \mathbf{x}_l - \mathbf{z}_l. \quad (11b)$$

where  $l$  is the index of the iteration (not to be confused with the index of time  $k$ ; there are several iterations within a given point in time); the initial value  $\mathbf{x}_0$  must be chosen by the

user. In general, we expect that Newton's method will converge locally and quadratically to a zero of  $\mathbf{f}$ . We now return to the non-linear constraint equation (8d). We use the chain rule of differentiation to compute the Jacobian of the function

$$\boldsymbol{\lambda} \rightarrow \mathbf{g}(\boldsymbol{\phi}_k(\boldsymbol{\lambda}))$$

and find that

$$\frac{\partial}{\partial \boldsymbol{\lambda}}(\mathbf{g} \circ \boldsymbol{\phi}_k)(\boldsymbol{\lambda}) = \mathbf{G}(\boldsymbol{\phi}_k(\boldsymbol{\lambda})) \frac{\partial \boldsymbol{\phi}_k}{\partial \boldsymbol{\lambda}}(\boldsymbol{\lambda}) = -h^2 \mathbf{G}(\boldsymbol{\phi}_k(\boldsymbol{\lambda})) \mathbf{M}^{-1} \mathbf{G}(\mathbf{q}_k)^T \quad (12)$$

which is why it is practical to define the matrix function  $\mathbf{A} : \mathbb{R}^{3s} \times \mathbb{R}^{3s} \rightarrow \mathbb{R}^{n \times n}$  given by

$$\mathbf{A}(\mathbf{x}, \mathbf{y}) := -h^2 \mathbf{G}(\mathbf{x}) \mathbf{M}^{-1} \mathbf{G}(\mathbf{y})^T. \quad (13)$$

In general, each matrix  $\mathbf{A}(\mathbf{x}, \mathbf{y}) = [a_{ij}]$  is both sparse and *structurally* symmetric because  $a_{ij} = a_{ji} = 0$  if the  $i$ th and  $j$ th bond do not share an atom<sup>12</sup>. We cannot expect that  $\mathbf{A}$  is symmetric in the sense that  $\mathbf{A} = \mathbf{A}^T$ , unless, of course,  $\mathbf{x} = \mathbf{y}$ .

Newton's method for solving equation (8d) with respect to the Lagrange multipliers  $\boldsymbol{\lambda}_k$  can be written as

$$\mathbf{A}(\boldsymbol{\phi}_k(\boldsymbol{\lambda}_{k,l}), \mathbf{q}_k^0) \mathbf{z}_{k,l} = \mathbf{g}(\boldsymbol{\phi}_k(\boldsymbol{\lambda}_{k,l})), \quad (14a)$$

$$\boldsymbol{\lambda}_{k,l+1} = \boldsymbol{\lambda}_{k,l} - \mathbf{z}_{k,l}, \quad (14b)$$

where  $\mathbf{q}_k^0 = \boldsymbol{\phi}_k(\boldsymbol{\lambda} = \mathbf{0})$  is the vector of atomic positions after applying the external forces of step  $k$  but before applying any constraint force. The initial value  $\boldsymbol{\lambda}_{k,0}$  in (14) is customarily  $\mathbf{0}$ . Eqs. (14) correspond to the system of equations which is also solved by SHAKE. ILVES-M and ILVES-F compute discrete approximations of the solution of the same system yet use different methods for solving the constraint equations. If the ILVES algorithms and SHAKE were all executed using exact arithmetic and if the constraint equations were solved exactly,

then these algorithms would all return the same results. This is because, if we assume that the Jacobian of the constraint function is of full rank, then the Inverse Function Theorem implies that the constraint equations have a unique solution when the time step is sufficiently small. Note that equations (14) correspond to a linear system of  $(n)$  equations that, for a given time  $t_k$ , must be solved in several iterations  $l$ . The linear system itself (Eq. (14a)), whose unknown is  $\mathbf{z}_{k,l}$  can be solved either directly or iteratively. The LINCS and P-LINCS algorithms<sup>2,13</sup> solve linear systems of the form  $(\mathbf{I} - \mathbf{B})\mathbf{x} = \mathbf{y}$  using a truncated Neumann series, i.e.,

$$\mathbf{x} = (\mathbf{I} - \mathbf{B})^{-1}\mathbf{y} = \sum_{j=1}^{\infty} \mathbf{B}^j \mathbf{y} \simeq \sum_{j=1}^R \mathbf{B}^j \mathbf{y}. \quad (15)$$

Their truncation order  $R$  is typically chosen to be 4 or 8. The Neumann series converges linearly at best as  $R$  tends towards infinity and there are physically relevant cases for which it does not converge at all<sup>2,13-15</sup>. Moreover, LINCS and P-LINCS usually fail when coupled angular constraints (e.g. for H-angles) are imposed<sup>16</sup>.

SHAKE converges locally and linearly with the number of iterations subject to very mild conditions<sup>17</sup>, whereas the truncation error introduced by LINCS converges linearly to zero as the truncation order  $R$  tends towards infinity provided that the spectral radius of  $\mathbf{B}$  is strictly less than 1. SHAKE and algorithms based on SHAKE’s design can also fail to converge, which is more likely when time steps or temperatures are high<sup>14,18</sup> or when external forces are either too strong<sup>15</sup> or lead to orthogonal directions of the bonds before and after applying them<sup>7</sup>. We expect that ILVES-M and ILVES-F will also suffer from this problem when the time step is sufficiently large. We do not believe that this problem can be addressed without the use of homotopy methods.

Apart from SHAKE, LINCS and P-LINCS, several algorithms to impose constraints on molecules have been proposed<sup>19-28</sup>. Among them we highlight the profusely cited RATTLE<sup>19</sup> and Settle<sup>20</sup>. The former enforces constraints for both positions and velocities, while the latter imposes constraints on water molecules treating them as rigid bodies. Other ones are typically slower than SHAKE<sup>22</sup> or have quadratic ( $\mathcal{O}(n^2)$ ) or cubic ( $\mathcal{O}(n^3)$ ) complexity<sup>23,24,26,27</sup>.

Some proposed constraint algorithms<sup>27,29,30</sup> rely on direct (*analytical*) solvers<sup>31</sup> for the involved linear systems of equations: M-SHAKE<sup>27</sup> performs Gaussian elimination without applying sparse techniques, resulting in a cubic ( $\mathcal{O}(n^3)$ ) numerical complexity in the number of constraints; MILC-SHAKE and MILCH-SHAKE<sup>29,30</sup> are only applicable to linear chains and n-alkanes, respectively. Application of sparse libraries for solving constraints, as well as parallel versions of SHAKE<sup>32,33</sup> have been proposed in the past<sup>11</sup>, yet not widely applied. Further algorithms have been designed to impose constraints on bond angles<sup>26,34,35</sup> and dihedral angles<sup>36,37</sup>. Refs.<sup>34,35</sup> use more sophisticated expressions than distance constraints for angular constraints, but solve the equations after each other (i.e. *à la SHAKE*, solving the first equation first, then the second equation, etc.). This way of proceeding converges slowly and is difficult to parallelize. The execution time of  $\theta$ -SHAKE<sup>34</sup> has the same order of magnitude as SHAKE's, which is significant for constraints on bond angles. Moreover, its efficiency relies on the low connectivity of the bonds of the tackled molecules. Though there are exceptions<sup>16,38–42</sup>, bond angles are not frequently constrained in MD simulations. This may be (at least in part) induced by the slowness of SHAKE for performing the corresponding calculations<sup>43</sup>, which is avoided by ILVES.

We now return our attention to Newton's method for computing the Lagrange multiplier. The central matrix  $\mathbf{A}(\phi_k(\lambda_{k,l}), \mathbf{q}_k^0)$  is a function of  $l$ , but it can be approximated by a constant matrix, i.e.,

$$\mathbf{A}(\phi_k(\lambda_{k,l}), \mathbf{q}_k^0) \approx \mathbf{A}(\mathbf{q}_k^0, \mathbf{q}_k^0) \quad (16)$$

simply because

$$\phi_k(\lambda) = \mathbf{q}_k + \mathcal{O}(h) \quad (17)$$

It is therefore natural to replace Newton's method with the iteration

$$\mathbf{A}(\mathbf{q}_k^0, \mathbf{q}_k^0) \mathbf{z}_{k,l} = \mathbf{g}(\phi_k(\lambda_{k,l})) , \quad (18)$$

$$\lambda_{k,l+1} = \lambda_{k,l} - \mathbf{z}_{k,l} \quad (19)$$



This approach is standard within the field of numerical analysis and different names such as the “simplified Newton method”<sup>44</sup> or the “chord method”<sup>45</sup> are used. It is the foundation of the Constant Constraint Matrix approach used by<sup>26</sup> in the context of molecular dynamics.

ILVES-M use local nonsymmetric approximations of the action of the inverse of each of the central matrices  $\mathbf{A}(\phi_k(\boldsymbol{\lambda}_{k,l}), \mathbf{q}_k^0)$ . ILVES-F use fixed local symmetric approximations of the inverse of the matrices  $\mathbf{A}(\mathbf{q}_k^0, \mathbf{q}_k^0)$ . If ILVES-M and ILVES-F are run until stagnation, then there is no significant difference between the computed Lagrange multipliers. However, ILVES-F is much faster than ILVES-M because the local approximations are symmetric and they are only computed and factored once per time step. In our tests, ILVES-F reaches the maximum attainable accuracy in a few iterations (5 or 6 iterations in a typical execution of **Gromacs** with floating point numbers in double precision and minimum tolerance, in contrast to the 3 or 4 iterations required by ILVES-M).

In addition to the ILVES algorithms presented in this paper, we tried a version of ILVES in which the directions of the constraint forces were allowed to change in every iteration; these directions were given by the bonds after the coordinates of every iteration were updated. We analysed the cases of updating  $\mathbf{A}$  for just some of the iterations as well. However, these methods provided no significant speedup, hence we do not present their results in the article. In addition, we tested several non-zero expressions for the starting guess used in the calculation of the Lagrange multipliers  $(\boldsymbol{\lambda}_{k,0})$ , though they did not provide further efficiency gains.

## Implementation

In this section, we describe the parallel implementation of ILVES-M and ILVES-F that we integrated into GROMACS. This implementation was used in all the calculations to analyse the performance and accuracy of the algorithm presented in this study. The implementation is fine-tuned for GROMACS, but it can be straightforwardly migrated—with the support of the authors of this study—to other predominant MD packages, such as NAMD<sup>46,47</sup>, AMBER<sup>48</sup>,

CHARMM<sup>49</sup>, LAMMPS or DESMOND.

In order to perform parallel calculations in a distributed memory environment, GROMACS divides the set of atoms being analyzed into distinct domains. Every time that GROMACS recomputes the neighbour list of atoms, the constraint algorithm is reinitialized to account for displacements of atoms between domains. The frequency of the recomputation of the neighbour list is controlled by GROMACS’ `nstlist` parameter, whose default value is 10 steps. Since the neighbour list is frequently recomputed, the performance of the initialization significantly affects the performance of the algorithm. Hence, we designed and implemented an initialization of ILVES, which minimizes the time spent in this stage.

ILVES-M and ILVES-F compute approximations of the corrections ( $\mathbf{z} = \mathbf{A}^{-1}\mathbf{g}$ , see the equations in the Supplemental Materials) needed for Newton’s method. They use three levels of parallelism: distributed memory parallelism, shared memory parallelism, and vectorization. To exploit distributed memory parallelism, our algorithm uses a natural extension of the Overlapping Partitioning Method (OPM)<sup>50</sup> from banded to general sparse systems. In distributed memory simulations with GROMACS, each domain also stores information about neighbouring atoms—those within a distance of up to  $I$  edges from any atom local to the domain, where  $I$  is a user-defined parameter (`lincs-order` in the case of P-LINCS). Using both the local and neighbouring atoms in each domain, a local approximation of the matrix-vector product  $\mathbf{z} = \mathbf{A}^{-1}\mathbf{g}$  is computed. This approximation is solved in each domain using a multi-thread implementation of Gaussian elimination based on the Schur method<sup>51</sup>. As detailed in the paragraphs that follow, this approach partitions the linear system, distributing segments across the domain’s threads for parallel processing. An example of the partitioning of a simple graph and the steps followed to solve its corresponding linear system is presented in Fig. S1.

The atoms and bonds handled by the constraint solver in each domain can be represented as an undirected graph  $G = (V, E)$ . The vertices  $V$  represent the atoms connected with at least one constrained bond and the edges  $E \subseteq V \times V$  represent the constrained bonds.

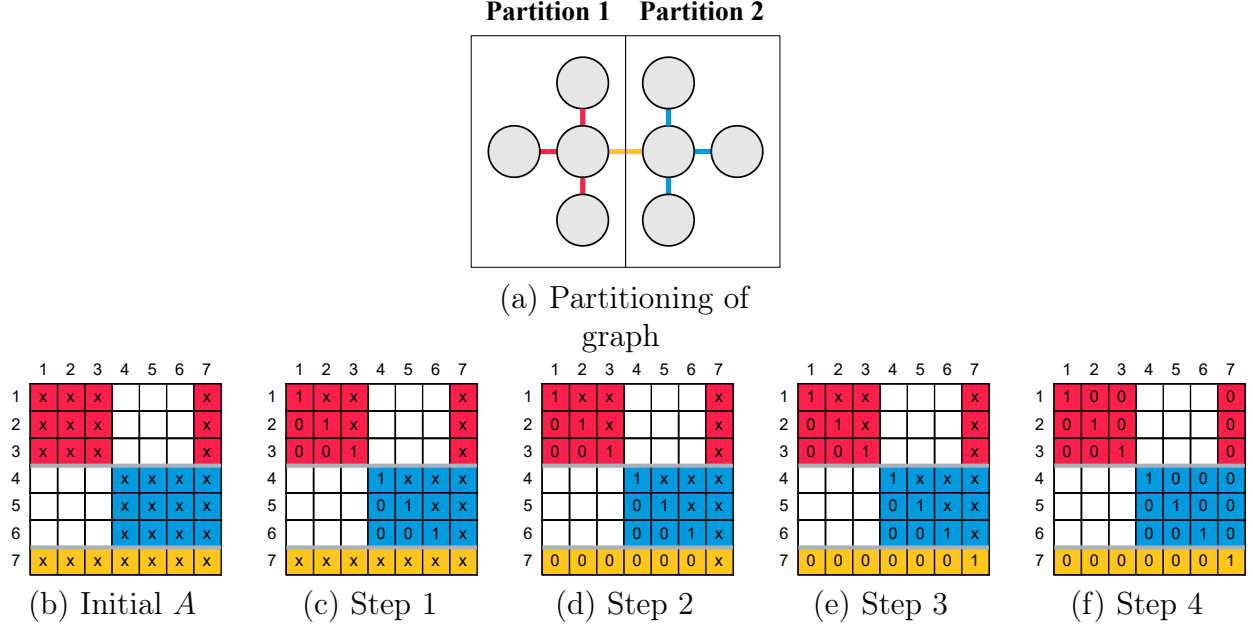


Figure S1: A possible partitioning of a simple graph (a), the corresponding coordinate matrix ( $\mathbf{A}$ ) of the linear system of equations ( $\mathbf{A}(\phi_k(\lambda_{k,l}), \mathbf{q}_k^0) \mathbf{z}_{k,l} = \mathbf{g}(\phi_k(\lambda_{k,l}))$ ) (b), and the steps to solve the linear system in parallel through Gauss-Jordan elimination and the Schur complement method (c-f). An analogous approach applies to solving the system with LU/LDLT decompositions and backward/forward substitution. Colours denote partitions, and each 'x' character represents a non-zero entry in the linear system. The red rows (1–3) and blue rows (4–6) represent private partitions for threads 1 and 2, respectively, while the yellow row (7) is the shared partition. To solve the system in parallel, each thread begins by zeroing the subdiagonal part of its private partition and setting the diagonal entries to ones (c). Next, the threads add their contributions to the shared partition in mutual exclusion (d). The master thread then performs Gauss-Jordan elimination on the shared partition (e), modifying only the last diagonal entry in this example. Once the master thread completes this step, all threads proceed in parallel to zero out the upper diagonal elements in their private partitions (f).

Since the simulation can contain more than one molecule and it is common to constrain only a subset of the bonds; for example, bonds that connect a hydrogen bond (H-bonds),  $G$  is usually a disconnected graph. From  $G$  we can compute its line-graph  $L(G)$  in which each vertex represents a constrained bond, and two constrained bonds are connected if they share one vertex in  $G$ . The adjacency matrix of the line-graph has the same sparsity pattern as the coordinate matrices of the linear systems solved by ILVES-M and ILVES-F.

The graph  $L(G)$  can be partitioned such that all the edges of  $L(G)$  that do not cross partitions comprise each thread’s private partition, while edges that connect vertices of  $L(G)$  which lie in different private partitions comprise the shared partition. The data in the private partitions can be processed simultaneously, as they are independent of one another. In contrast, the data in the shared partition must be processed separately, in mutual exclusion from the private partitions, to ensure correctness and avoid conflicts.

While both P-LINCS and ILVES-M/F employ a partitioning of  $L(G)$  for parallel execution, their methodologies differ significantly. P-LINCS partitions  $L(G)$  directly dividing its vertices into roughly equal sets, followed by computation to identify edges crossing partitions. On the other hand, ILVES-M/F tries to minimize the edges crossing partitions using a greedy algorithm to partition  $G$  rather than  $L(G)$ . Graphs in MD exhibit very low connectivity and, additionally, GROMACS assigns close indexes to connected atoms. Our algorithm sequentially assigns vertices of  $G$  to partition  $p$  while the partition size remains below a target value plus an offset. The final vertex in partition  $p$  is chosen based on the number of edges cut and the similarity of the partition size to the target size. This greedy algorithm runs in  $\mathcal{O}(|E|)$  time, where  $|E|$  is the number of edges in  $G$ , and produces partitions comparable to those generated by general but slower graph-partitioning libraries like METIS<sup>52</sup>, often cutting a similar or smaller number of edges relative to the number of partitions. Our partitioning approach produces significantly fewer cuts than P-LINCS’, which results in notably less serial work and less synchronization between threads in cases where zero-cut partitions are possible, such as simulations of several small molecules.

The pseudocode of our greedy approach for partitioning a graph into  $k$  partitions is presented in Fig. S2. For the results discussed in this study, the parameter `maxDeviation` was set to 0.05, and `cutPenalty` was assigned a value of 10.

After computing the partitioning of  $L(G)$  we use a modified parallel implementation of the Approximate Minimum Degree ordering algorithm (AMD)<sup>53</sup> to minimize the fillins in the part of the linear system corresponding to each partition (a *fillin* is a zero entry of the coordinate matrix which becomes non-zero when computing a factorization such as an LU or an LDLT factorization which is needed for Gaussian elimination). This step completes the initialization of the ILVES algorithm, which is then ready to apply the constraints in each step until reinitialization is required after GROMACS recomputes its neighbour list.

ILVES-M and ILVES-F enforce constraints at each step through three primary phases: i) constructing the relevant linear systems and calculating the maximum relative error, ii) solving the linear systems, and iii) updating atomic positions. These phases are iteratively executed until the desired tolerance for the maximum relative error is reached.

During the first phase, each thread constructs the corresponding portion of the linear system for its private partition, while the master thread also handles the shared partition. In this phase, the private and shared partitions can be computed concurrently. The computation of the maximum relative error is overlapped with the construction of the linear system. In distributed memory simulations, domains exchange their maximum relative errors after this step is complete. Note that for ILVES-F, the coordinate matrix of the linear system of equations to solve ( $\mathbf{A}$ ) remains constant for all iterations and is thus computed just once per simulated time. This step is vectorized using the GROMACS SIMD intrinsics interface.

Next, the Lagrange multipliers  $\boldsymbol{\lambda}$  are calculated by solving the linear system in parallel through LU (LDLT) factorization for ILVES-M (ILVES-F). The factorization is followed by forward and backward substitutions. ILVES-F requires a single LDLT factorization per step because  $\mathbf{A}$  remains unchanged for all the iterations in a given simulated time. This process is detailed in Fig. S1.

Figure S2: Greedy K-way Partitioning of a Graph

---

**Require:**  $k$ : number of partitions,  $neighs$ : sorted adjacency list where  $neighs[v]$  contains the list of neighboring vertices for vertex  $v$ .

**Ensure:** Array  $ids$  with the partition ID of each vertex.

```

1: Initialize  $maxDeviation$  and  $cutPenalty$  as problem-specific constants
2:  $ids \leftarrow$  vector of size  $|neighs|$ , initialized to  $-1$ 
3:  $v \leftarrow 0$ 
4: for  $p \leftarrow 0$  to  $k - 1$  do
5:    $targetPsize \leftarrow (|neighs| - v) / (k - p)$ 
6:    $maxPsize \leftarrow targetPsize \times (1 + maxDeviation)$ 
7:    $bestVertex \leftarrow -1$ 
8:    $bestScore \leftarrow \infty$ 
9:    $psize \leftarrow 0$ 
10:   $ncuts \leftarrow 0$ 
11:  while  $v < |neighs|$  and  $psize \leq maxPsize$  do
12:    if  $ids[v] = p$  then
13:       $ncuts \leftarrow ncuts - 1$ 
14:    else
15:       $ids[v] \leftarrow p$ 
16:    end if
17:     $psize \leftarrow psize + 1$ 
18:     $i \leftarrow \text{BinarySearch}(v, neighs[v])$ 
19:    for  $neigh$  in  $neighs[v]$  from index  $i + 1$  onward do
20:      if  $ids[neigh] < p$  then
21:         $ids[neigh] \leftarrow p$ 
22:         $ncuts \leftarrow ncuts + 1$ 
23:      end if
24:    end for
25:     $score \leftarrow |psize - targetPsize| + ncuts \times cutPenalty$ 
26:    if  $score < bestScore$  then
27:       $bestVertex \leftarrow v$ 
28:       $bestScore \leftarrow score$ 
29:    end if
30:     $v \leftarrow v + 1$ 
31:  end while
32:   $v \leftarrow bestVertex + 1$ 
33: end for
34: for  $v \leftarrow v$  to  $|neighs| - 1$  do
35:    $ids[v] \leftarrow k - 1$ 
36: end for
37: return  $ids$ 

```

---

Finally, the positions of the atoms are updated. Updates to the positions of atoms in private partitions are processed in mutual exclusion to updates of atoms in the shared partition. In distributed memory simulations, the updated atomic positions are exchanged between domains, ensuring that each domain has the latest positions of its neighboring atoms.

## Experimental Setup

Table S1: Main features of the computing nodes used to execute the simulations.

Processor	$2 \times$ Intel Xeon Platinum 8480+
Cores	$2 \times 56$
Frequency	2 GHz
L1i cache (I + D)	32 KB + 48 KB (per core)
L2 cache	2 MB (per core)
LLC	105 MB (shared)
Main Memory	256 GB DDR5 ( $16 \times 16$ GB 4800 MHz DIMMs)
Interconnection	ConnectX-7 NDR200 InfiniBand (100 Gb/s per node)

The simulations presented in this text were performed on a multi-node cluster. Each node is equipped with two Intel Xeon Platinum 8480+ chips, each with 56 cores. The primary features of the nodes are summarized in Tab. S1.

We used GROMACS 2021.0 compiled with GCC-10.1.0 for the experiments. All of the results presented in the main article were obtained with GROMACS compiled in double-precision mode (`-DGMX_DOUBLE=on`).

To ensure a fair comparison of the algorithms, we generated a modified version of the P-LINCS implementation of GROMACS, allowing us to set the desired tolerance as in the case of the SHAKE and ILVES algorithms. This was accomplished by repeating P-LINCS' correction phase, controlled by the `lincs-iter` parameter in the original implementation until the desired error is met. This modified version is referred to as MP-LINCS throughout the text. Although this modification introduces additional synchronization

points in parallel executions, potentially affecting performance, it is important to note that it is straightforward to modify ILVES to execute a fixed number of iterations without checking the tolerance, sparing the same synchronization points introduced in MP-LINCS.

## Simulations

Table S2: Molecular systems simulated in this article. In the force field column, C22+CMAP is Charmm22+CMAP, C36m is Charmm36m and C36 is Charmm36.

<b>System</b>	<b># Molec. entities (PDB ID)</b>	<b># Mol.</b>	<b># Resid./ Atoms</b>	<b># Constr. all-bonds/ H-bonds</b>	<b>Force Field/ Water Model</b>
Solvated barnase <sup>54</sup>	barnase (1A2P)	1	108/1705	1721/836	C22+CMAP <sup>55</sup>
	Water	62848	188544	—	Tip3p <sup>56</sup>
	NA <sup>+</sup> , Cl <sup>-</sup>	4/11	15	—	C22+CMAP <sup>55</sup>
Solvated nuclease <sup>57</sup>	nuclease (2SNS)	1	149/2398	2459/1224	C22+CMAP <sup>55</sup>
	Water	115602	346806	—	Tip3p <sup>56</sup>
	Cl <sup>-</sup>	10	10	—	C22+CMAP <sup>55</sup>
Solvated COVID <sup>58</sup> protease	protease (5R7Y)	1	304/4645	4697/2297	C22+CMAP <sup>55</sup>
	Water	61958	185874	—	Tip3p <sup>56</sup>
	NA <sup>+</sup> , Cl <sup>-</sup>	8/4	12	—	C22+CMAP <sup>55</sup>
Pure benzene <sup>59</sup>	benzene	2000	24000	24000/12000	Gromos54a7 <sup>60</sup>
Solvated DNA- proteins <sup>61</sup>	histones (3LEL)	16	1540/25257	25933/13078	ff19SB <sup>62</sup>
	DNA	4	588/18712	20178/6670	OL21 <sup>63</sup>
	Water	83872	251616	—	OPC4 <sup>64</sup>
	NA <sup>+</sup>	428	428	—	ff19SB <sup>62</sup>
Aquaporin 1 embedded in lipid bilayer <sup>65</sup>	Aqp1 (1J4N)	4	996/15072	15480/7755	C36m <sup>66</sup>
	MMPC	1129	133222	131837/81193	C36 <sup>67</sup>
	Water	80598	241794	—	Tip3p <sup>56</sup>
	NA <sup>+</sup> , Cl <sup>-</sup>	223/235	458	—	C36 <sup>67</sup>

We conducted simulations on a diverse set of molecular systems, including three solvated proteins, a solvated protein-DNA complex, an organic solvent and a membrane protein embedded in a lipid bilayer surrounded by water. Tab. S2 summarizes the key characteristics of the systems, while Fig. S3 provides a visual representation. Biological macromolecules, like



DNA and proteins, present well-known interest for medical and biotechnological purposes. Benzene, as a representation of small molecules, has important chemical and industrial applications<sup>68</sup>. Proteins embedded in a lipid bilayer include channels, transporters, and signal receptors, among others, all of which play a vital role in cell biology and medical research<sup>69</sup>. Along with the diversity of this molecular representation, the inclusion of small, medium and large systems (e.g., the protein/membrane system containing 390k atoms), enabled us to evaluate the performance of our ILVES algorithms across a wide range of molecular systems and sizes.

Below we outline the procedures on which the simulations are based. All the systems, except the protein (human aquaporin-1) embedded in a lipid bilayer, were prepared through a standard protocol involving solvation, minimization, heating, and equilibration. The most important parameters used in the preparation and also in the production phase of the simulations are listed in Tab. S3. The membrane protein system was prepared using the membrane-builder wizard from the CHARMM-GUI online tool<sup>70-73</sup>. We used different force fields for the simulations (Tab. S2), and explicit Tip3p water molecules<sup>74</sup> were used to solvate the macromolecular systems, except for the protein-DNA complex, which was solvated with the OPC4 water model<sup>75</sup>. The ionizable residues of proteins were protonated at pH 7 (GROMACS default), except for the case of barnase, which was set to pH 4.1 because the experimental thermodynamic observables used as a control were obtained under this condition. Chloride and/or sodium ions were added to neutralize the systems or to achieve the desired ionic strength. A cubic box was used for the membrane system, while a truncated dodecahedral box was used for the rest of the systems. The Verlet cutoff scheme<sup>9,76</sup> was applied for van der Waals interactions, and the Particle Mesh Ewald (PME) method<sup>77</sup> was used to account for electrostatics. Both methods were used with a radius cutoff of 1.0 nm (0.9 nm for the membrane protein), while all the preparation steps imposed periodic boundary conditions (PBC).

The minimization step was performed using the steepest descent algorithm<sup>78</sup>, followed by

Table S3: Relevant input parameters employed in the stages of the simulations.

Step	General settings	PBC & Constraints	Thermodynamic Ensemble (baths)	Physical Conditions	Time step / Simulated Time
Min.	Integrator: steepest descent Neighboring searching: grid rcoul (PME): 1.0 (0.9) <sup>b</sup> nm rvdw (cut-off): 1.0 (0.9) <sup>b</sup> nm	PBC: xyz Constr: none	—	Emtol: 1 kJ/mol Temp: 0 K Press: 0 atm	max 20K steps
Heating	Integrator: md Neighboring searching: grid rcoul (PME): 1.0 (0.9) <sup>b</sup> nm rvdw (cut-off): 1.0 (0.9) <sup>b</sup> nm vdw-mod: potential-shift-verlet	PBC: xyz Constr: all-bonds	Termost: Berendsen $\tau_T = 0.1$ ps	Temp: Ini-T + ramp ( $n \times 50$ K) Press: 0 atm	1 fs / $n \times 50$ ps
Equil. 1	Same as Heating	Same as Heating	NVT Termost: v-rescale $\tau_T = 0.1$ ps	Temp: Final-T Press: 0 atm	1 fs / 100 ps
Equil. 2	Same as Heating	Same as Heating	NPT Termost: v-rescale $\tau_T = 0.1$ ps Barost: Berendsen $\tau_P = 2.0$ ps	Temp: Final-T Press: 1 atm	2 fs / 100 ps
Equil. 3	Same as Heating	Same as Heating	NPT Termost: v-rescale $\tau_T = 0.1$ ps Barost: Parrinello-Rahman $\tau_P = 2.0$ ps	Same as Equil. 2	2 fs / 200 ps
Prod.	Same as Heating	PBC: xyz Constr: all-bonds, h-bonds or h-angles	Same as Equil. 3	Same as Equil. 2	2 fs / 0.1 ns or 2 ns

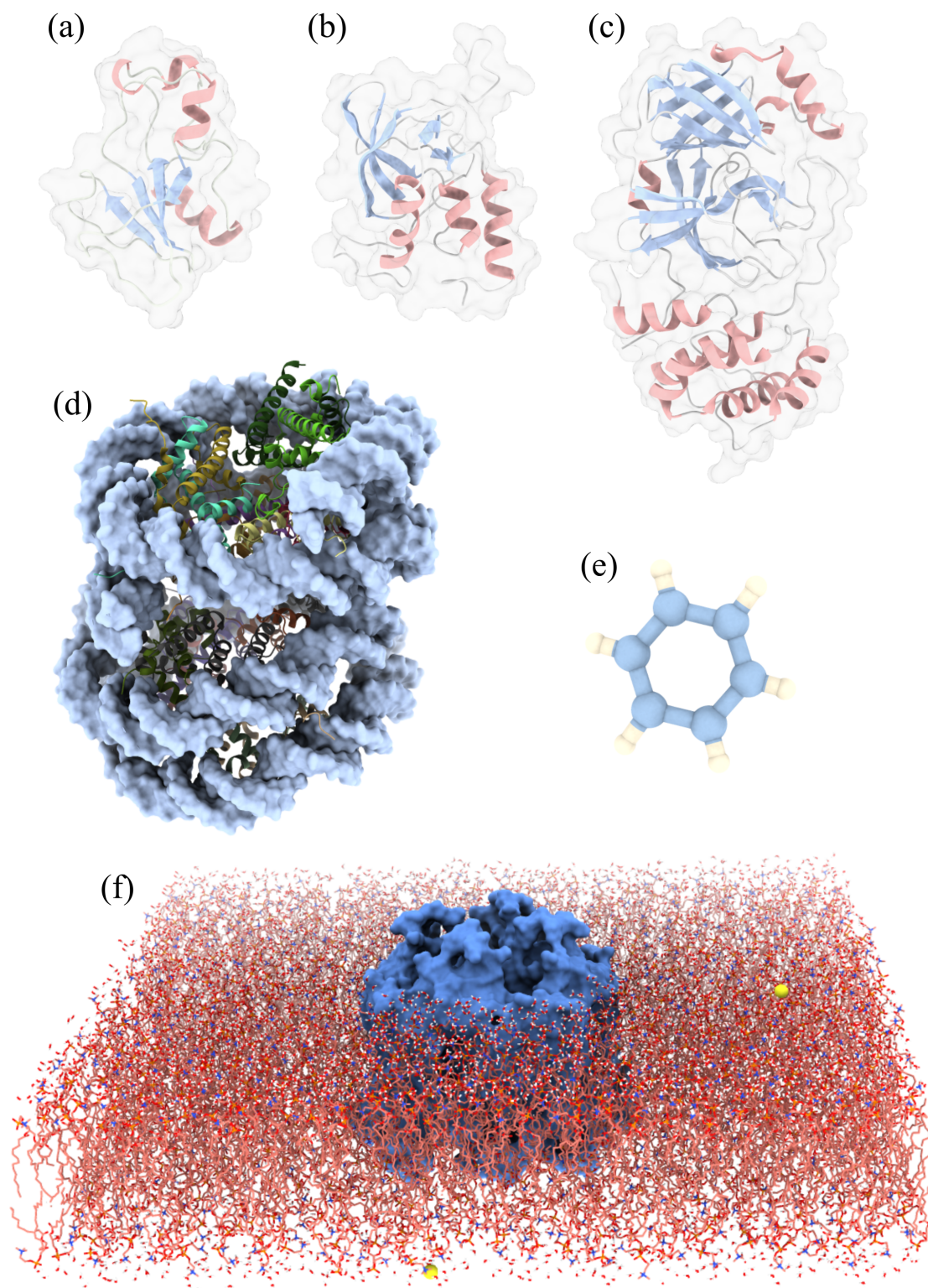


Figure S3: Representations of the simulated molecules, covering solvated proteins: (a) barnase (PDB 1A2P), (b) nuclease (PDB 2SNS) and (c) Covid-19 main protease (PDB 5R7Y); (d) a solvated protein-DNA complex (PDB 3LEL); (e) an organic solvent (benzene); and (f) a tetrameric protein embedded in a lipid bilayer.

an NVT gradual heating protocol, increasing temperature by 50 K every 50 ps with a 1 fs time step, until the target temperature was reached. The equilibration process began with a 100 ps NVT simulation with a 2 fs time step using the V-rescale thermostat<sup>79</sup> ( $\tau_T = 0.1$  ps). During this step, position restraints were applied to all the heavy atoms (protein, DNA, lipids, and water). This was followed by a 100 ps simulation in the NPT ensemble using a 2 fs time step and the heavy atoms now unrestrained. V-rescale thermostat ( $\tau_T = 0.1$  ps) and the Berendsen barostat<sup>80</sup> ( $p = 1$  atm,  $\tau_P = 2.0$  ps) were settled. Finally, the system underwent 200-ps NPT simulation with a 2 fs time step, employing the V-rescale thermostat ( $\tau_T = 0.1$  ps) and the Parrinello-Rahman barostat<sup>81</sup> ( $p = 1$  atm,  $\tau_P = 2.0$  ps). Temperature corrections due to the thermostat were applied every 10 steps (GROMACS' `nsttcouple` default value). Input files from our simulations can be retrieved from the provided GitHub repository ([https://github.com/LorienLV/\\_PAPER\\_ILVES](https://github.com/LorienLV/_PAPER_ILVES)). The final equilibrated configuration served as the starting point for the production phase of the simulations, which are analyzed in the following sections.

## Reliability study

In a previous work<sup>82,83</sup>, one of the authors presented an MD-based method that has proven accurate in reproducing protein folding thermodynamics using both SHAKE and P-LINCS. In this paper, we applied that approach to evaluate the reliability of our constraint solvers by calculating three thermodynamic observable quantities: namely, the change in enthalpy upon unfolding  $\Delta H_{unf}$  (or upon folding, with opposite sign); the change in heat capacity upon the same event,  $\Delta C_{p_{unf}}$ ; and the corresponding change in Gibbs free energy (i.e., the protein conformational stability),  $\Delta G_{unf}$ . The analysis was conducted by simulating two well-studied proteins, barnase and nuclease (Tab. S2), which have similarly been modelled in Refs.<sup>82,83</sup>. In Tab. S3, we include the main parameters used in the preparation and production simulations carried out with these systems.

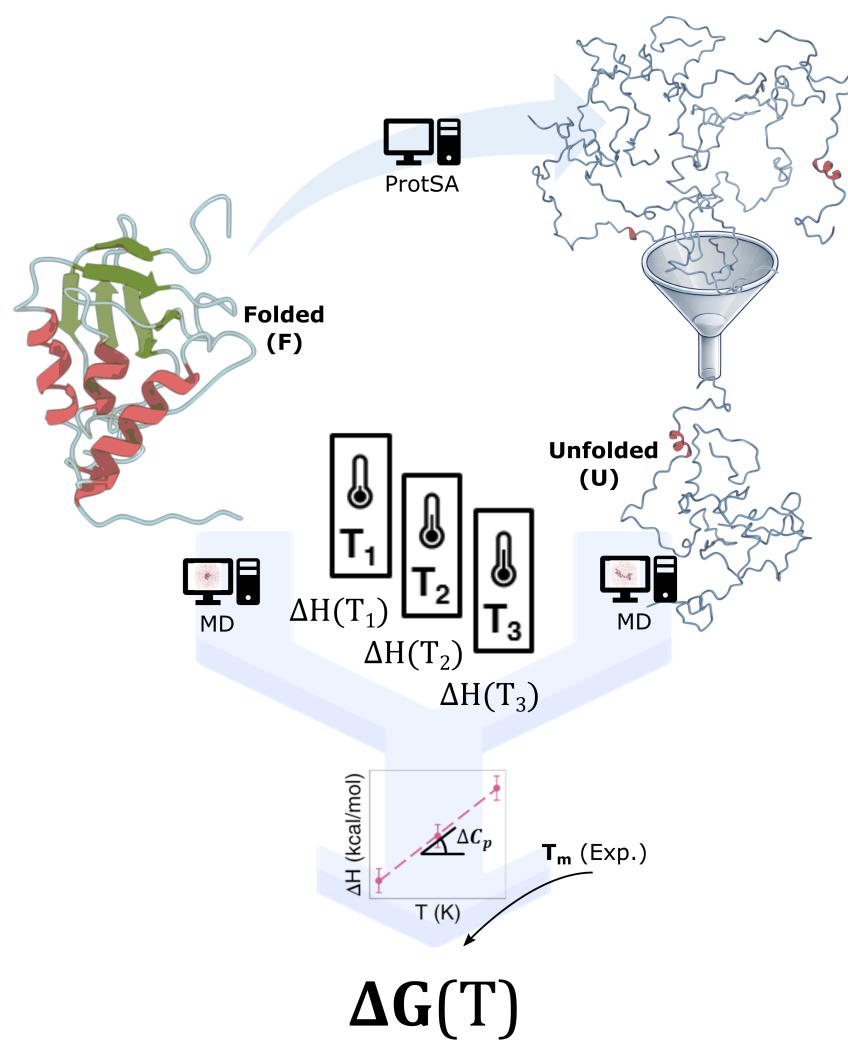


Figure S4: Workflow of the calculation of observable quantities.

The referred method<sup>82,83</sup> primarily involves separately simulating—in the NPT ensemble—the folded and unfolded states of a solvated protein (see Fig. S4) under identical conditions (force field, type and number of water molecules, ions, pH, temperature, pressure, time step, simulation length, etc.). To achieve precise averaging of thermodynamics quantities, the method requires representative sampling of the conformational space of both states: we used 40 simulation replicas for the folded state and 100 replicas for the unfolded state, both lasting 2 ns, with a time step of 2 fs. The 100 protein structures representative of the unfolded state are a filtered sample of a larger set of completely unfolded conformations generated by the ProtSA server<sup>84</sup>. The average enthalpies obtained for the two states are subtracted to yield the enthalpy change upon unfolding,  $\Delta H_{unf}$ . From this calculation, the error (standard error of the mean, as given in the table of the main article) is obtained as the sum of both errors: that corresponding to the folded ensemble and that of the unfolded ensemble. The calculation of  $\Delta H_{unf}$  is performed for three temperatures (295 K, 315 K, and 335 K) allowing the determination of the enthalpy change with temperature, which is typically linear. This linear relationship, whose slope corresponds to the change in heat capacity,  $\Delta C_{p_{unf}}$ , allows interpolating the enthalpy change at the mid denaturation temperature ( $T_m$ , taken from the literature), which is the enthalpy change that is commonly reported in scientific articles. The reported error in  $\Delta C_{p_{unf}}$  calculation (Tab. of the main article) is that obtained from the linear fitting. Once these two thermodynamic quantities are calculated ( $\Delta H_{unf}$  at the  $T_m$  and  $\Delta C_{p_{unf}}$ ), the Gibbs free energy change can be obtained through the Gibbs-Helmholtz equation<sup>85</sup>:

$$\Delta G(T) = \Delta H_m \left(1 - \frac{T}{T_m}\right) - \Delta C_p \left[T_m - T + T \ln \left(\frac{T}{T_m}\right)\right]. \quad (20)$$

The reported error in  $\Delta G(T)$  calculations (Tab. of the main paper) is obtained by error propagation. In this assessment, we used the combination of force field and water model that has been shown to best reproduce experimental protein thermodynamics<sup>82,83</sup>: Charmm22+CMAP<sup>55</sup> and Tip3p<sup>56</sup>.

## ILVES’ foundations

In Ref.<sup>86</sup> we pointed out a misconception appearing in numerous publications regarding constrained MD, which wrongly assumes that applying direct solvers to the linear systems (see Eq.( 14a)) has cubic numerical complexity; that is, if  $n$  is the number of constraints, then explicit Gaussian elimination requires  $\mathcal{O}(n^3)$  floating point operations. We proved that many real molecules exist for which Gaussian elimination could be completed using  $\mathcal{O}(n)$  rather than  $\mathcal{O}(n^3)$  arithmetic operations. The reduction is due to the fact that many molecules, such as proteins and nucleic acids, have a geometry that is essentially linear. Therefore, if the bonds are numbered sequentially from one end of the molecule to the other, the relevant matrices are banded<sup>87</sup> and sparse within the band.

Later, we investigated how to improve the efficiency of direct solvers, which we applied to calculate constraint forces, finding that compiled (loop-free) code, task fusion, and vectorization reduced execution times using small-molecule test cases for a proof-of-concept<sup>88</sup>. We then analysed how the Constant Constraint Matrix method<sup>26</sup> could be applied to direct solvers<sup>89</sup>, finding that the use of symmetric coordinate matrices in linear systems still showed rapid linear convergence to the solution.

Afterwards, we implemented ILVES-PC, a proof-of-concept which solves constraints for some simulated systems faster than the state-of-the-art<sup>12</sup>. This algorithm is based on the usage of compiled (loop-free) code, which takes advantage of the fact that the building blocks of peptides and proteins (residues of amino acids) follow a limited set of predefined patterns. This research also illustrated the capabilities of compiled code applied to molecular simulation. In<sup>12</sup>, we also investigated the impact of the accuracy for solving constraint equations on the dynamics of the simulated systems, finding that the default of **Gromacs** (tolerance for the relative error of the constraints equal to  $10^{-4}$ ) leads to non-negligible errors (which manifest as relatively large drifts of the energy in NVE simulations and of the conserved quantity in NPT simulations). In<sup>90</sup>, we further explore why constraints should be solved as accurately as possible.

This document presents ILVES-M and ILVES-F, two parallel constraint solvers based on direct solvers which are faster (for equal accuracy) than the state-of-the-art (SHAKE, P-LINCS) and which can efficiently impose constraints on bond angles. This implementation is expected to be a valuable tool for the community of researchers in molecular simulation.

## Further discussion about the need for accuracy when solving constraint equations

If the constraint equations are solved exactly, then the SHAKE algorithm is second-order accurate in the time step. In practice, it is impossible to solve the constraint equations exactly and we accept an approximation if the relative error is less than the tolerance  $Tol$  passed to the constraint solver. In this section, we shall explain why the only safe value of  $Tol$  is tiny and why we should run the constraint solver until stagnation. We shall present arguments that should appeal to both to the numerical analyst and to the experimental scientist who seek to validate a model of the physical reality.

### Are the computed numbers behaving as they should?

It is important to distinguish between the exact numbers that are defined by the SHAKE algorithm and the numbers that are computed when the algorithm is executed using finite precision arithmetic and tolerance  $Tol > 0$ .

We begin by demonstrating that if the tolerance  $Tol$  is small enough, then the computed numbers behave in a manner that is indistinguishable from the numbers that are defined by the SHAKE algorithm. To this end, we shall study a simple pendulum. This is a standard test problem. The necessary files to execute the experiments and regenerate our figures from scratch can be found in the public GitHub repository



Table S4: Parameters defining a simple pendulum.

Parameter	Symbol	Value
Mass	$m$	1 $kg$
Length	$l$	1 $m$
Gravitational const.	$g$	9.82 $m/s^2$
Initial velocity	$v_0$	(1, 0) $m/s$
Initial position	$r_0$	(0, 0)

[https://github.com/spockcc/\\_PAPER\\_ILVES\\_pendulum](https://github.com/spockcc/_PAPER_ILVES_pendulum)

We shall demonstrate that if the tolerance in solving is small enough, then the total energy is very nearly preserved and the error is  $\mathcal{O}(h^2)$ . Our pendulum is defined by Tab. S4.

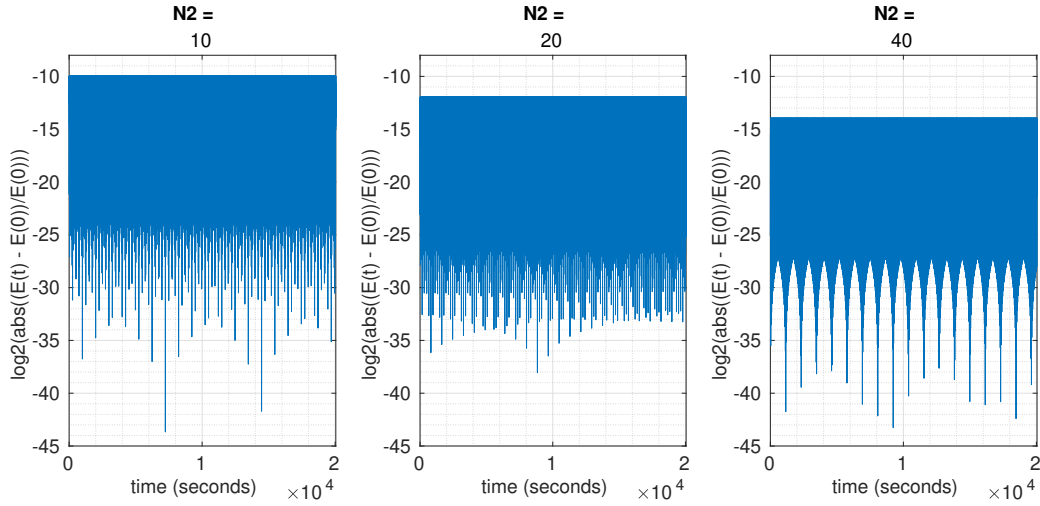


Figure S5: Total energy of a simple pendulum as a function of time for three different values of timestep.

The MATLAB function `shake_pendulum` is included in the GitHub mentioned above. It does a sequence of 3 simulations of the same pendulum using different values of the time step and generates Fig. S5. The exact parameters of these simulations are given by Tab. S5.

We note that the simulations do  $n_{sp} \cdot N2 \in \{100, 200, 400\}$  steps per period, which is far above the rule of thumb that suggests at least 5 steps per period. In Fig. S5 we see that the relative error of the total energy, i.e.,

$$R(t) = \frac{E(t) - E(0)}{E(0)} \quad (21)$$

Table S5: The parameters for the first set of simulations of the pendulum given by Tab. S4. The evolution of the total energy is shown in Fig. S5.

Description	Name	Value
Number of periods	<b>np</b>	10,000
Number of recorded state vectors per period	<b>nsp</b>	10
Number of recorded state vectors	<b>N1</b>	$N1 = np \cdot nsp$
Number of steps between recorded state vectors	<b>N2</b>	$\{10, 20, 40\}$
Tolerance passed to constraint solver	<b>Tol</b>	$10^{-12}$

is bounded as a function of the time  $t$  and that the maximum value of the absolute value of relative error is approximately  $\{2^{-10}, 2^{-12}, 2^{-14}\}$  for  $N2 = \{10, 20, 40\}$ . This is experimental evidence in support of the hypothesis that the maximum relative error is  $\mathcal{O}(h^2)$ . This is the behaviour that we would observe if the algorithm were executed using exact arithmetic and the constraint equations were solved exactly.

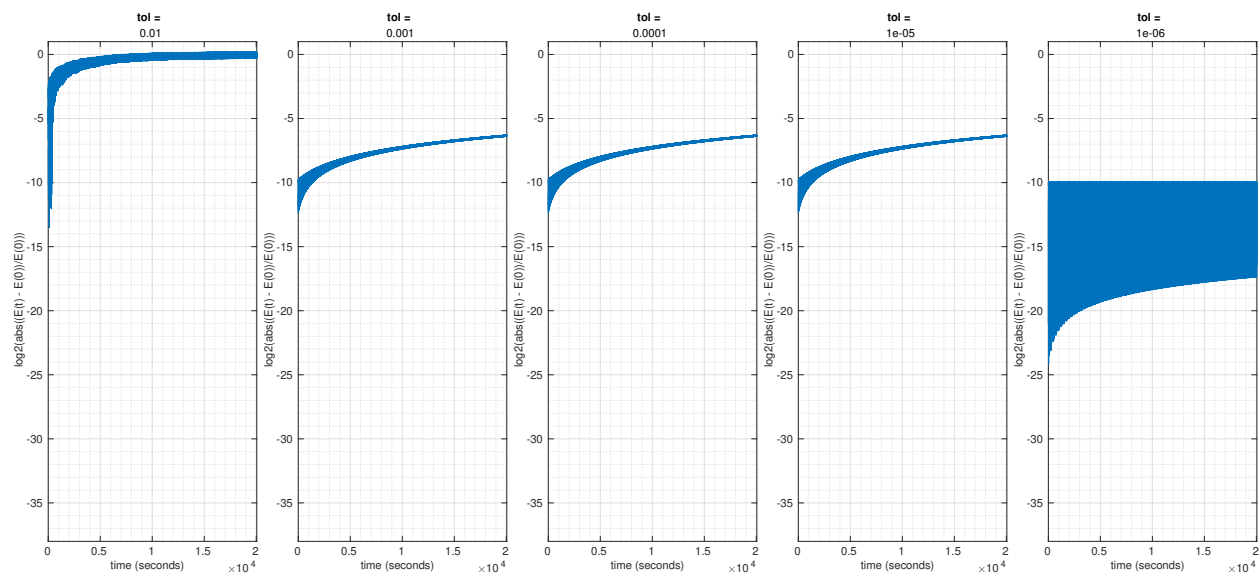


Figure S6: The evolution of the total energy of a pendulum over time for different values of the tolerance Tol passed to the constraint solver.

The MATLAB function `shake_pendulum` does a second sequence of 10 simulations of the same pendulum using different values of the tolerance Tol. The exact parameters are given by Tab. S6. The constraint solver is a quasi-Newton method, specifically the simplified Newton method that uses a fixed value of the Jacobian for each step. The linear convergence

Table S6: The parameters for the second set of simulations of a pendulum given by Tab. S4. The evolution of the total energy is displayed in Fig. S6.

Description	Name	Value
Number of periods	<b>np</b>	10,000
Number of recorded state vectors per period	<b>nsp</b>	10
Number of recorded state vectors	<b>N1</b>	<b>N1 = np · nsp</b>
Number of steps between recorded state vectors	<b>N2</b>	10
Tolerance passed to constraint solver	<b>Tol</b>	$\{10^{-2}, 10^{-3}, \dots, 10^{-6}\}$
Constraint solver	<b>method</b>	<b>quasi</b>

of this method ensures that the constraints are solved with a relative error that is essentially equal to the tolerance passed to the solver. Fig. S6 shows how the relative error  $R(t)$  of the energy evolves over time for different values of the tolerance Tol. In particular, we see that relative error is a strictly increasing function of  $t$  for Tol  $\in \{10^{-2}, 10^{-3}, 10^{-4}, 10^{-5}\}$ . For these values of the tolerance Tol, we cannot claim that the simulation corresponds to an isolated system because the fundamental principle of the conservation of energy is clearly violated. However, for  $\tau = 10^{-6}$ , the maximum relative error is bounded as a function of  $t$ . Again, this is exactly the behaviour we would observe if the algorithm were executed in exact arithmetic and the constraint equations were solved exactly.

These two numerical experiments show that if the tolerance Tol is sufficiently small, then the total energy of the pendulum is very nearly preserved, and the computed numbers behave in a manner that is consistent with a method that is second order accurate in the time step. If the tolerance is not sufficiently small, then the absolute value of the relative error of the energy is an increasing function of time.

In the absence of a complete understanding of the relationship between the system, the time step, the tolerance and the evolution of the relative error of the energy, the only safe policy is to run the constraint solver until it stagnates due to the limitation of finite precision arithmetic. Naturally, this process is not practical unless the constraint solver converges rapidly.

The MATLAB function `shake_pendulum` also conducts a third sequence of experiments.

Table S7: The parameters of a third set of simulations of the pendulum given by Tab. S4. The results are shown in Fig. S7.

Parameter	Name	Value (s)
Number of periods	<code>np</code>	10,000
Number of recorded state vectors per period	<code>nsp</code>	10
Number of recorded state vectors	<code>N1</code>	$N1 = np \cdot nsp$
Number of steps between recorded state vectors	<code>N2</code>	10
Tolerance passed to constraint solver	<code>Tol</code>	$10^{-4}$
Constraint solver	<code>method</code>	<code>{newton,quasi}</code>

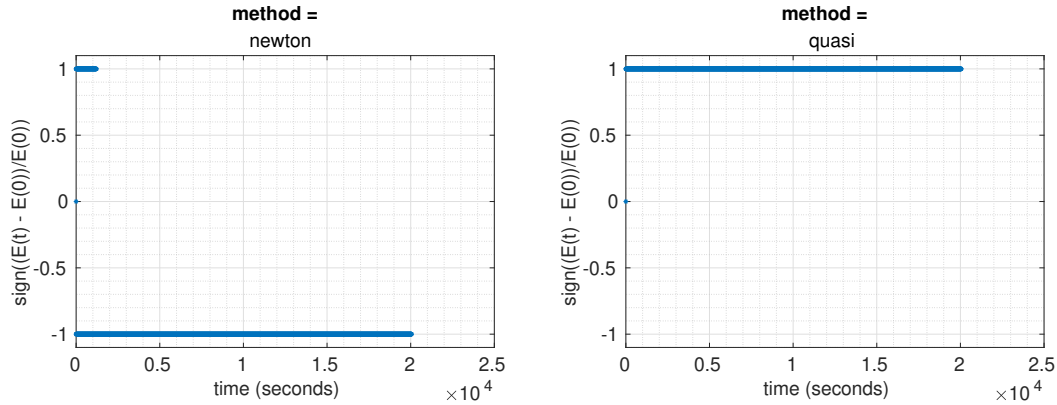


Figure S7: Sign of the relative error of the total energy for pendulum for two different constraint solvers as a function of the time: Newton's method (left) and the simplified Newton method (right).

Here, the focus is on the sign of the relative error rather than its absolute value. The two experiments reveal that the sign of the relative error can depend on the choice of the constraint solver! The exact parameters of these simulations are given by Tab. S7.

Fig. S7 shows the evolution of the sign of relative error of the energy. The scientist who uses Newton's method to probe the inner mysteries of the pendulum will (almost certainly) conclude that the system loses energy over time, whereas the scientist who uses the simplified Newton method will conclude that the system gains energy over time. It is intolerable that the physical conclusions drawn from a numerical experiment might depend on the algorithm used to solve certain central equations.

### Can we validate our model of reality?

We shall now argue further in favour of solving the constraint equations as accurately as the hardware allows. To this end, we ask the reader to consider a fundamental question: What is the purpose of an MD simulation? In general, we seek to obtain numbers that cannot be measured in the laboratory either because we lack the equipment or because the procedure is too expensive. But before these experiments can be conducted it is necessary to validate our model and determine if it accurately captures critical aspects of the physical reality. In general, we do not care for the solution of a specific initial value problem for the system of differential algebraic equations (DAEs); rather we seek the value of a physical quantity that can be computed in terms of several such trajectories. Let  $T$  denote the value that would be obtained if we could solve the relevant systems of DAEs exactly. Let  $A_h$  be the value that would be obtained if we could solve the corresponding discrete-time equations exactly and let  $\hat{A}_h$  denote the value of  $A_h$  that is returned by the computer. It is important to recognise that the three numbers  $T$ ,  $A_h$  and  $\hat{A}_h$  are almost certainly different. The discretization error  $T - A_h$  is not zero because we have replaced the system of DAEs with a set of discrete equations. The computational error  $A_h - \hat{A}_h$  is not zero because we

cannot solve the constraint equations exactly (truncation error) and because we are forced to use finite precision arithmetic (rounding error). Why should we care about these errors? We validate our model by comparing  $T$  against the physical reality  $P$ . We cannot compute  $T$  directly, and a small value of the observed error  $P - \hat{A}_h$  does not necessarily imply that the modelling error  $P - T$  is small. Why is that? This issue can be understood using the elementary identity

$$\underbrace{(P - T)}_{\text{modelling error}} = \underbrace{(P - \hat{A}_h)}_{\text{observed error}} - \underbrace{(A_h - \hat{A}_h)}_{\text{computational error}} - \underbrace{(T - A_h)}_{\text{discretization error}} . \quad (22)$$

From this identity we conclude that  $T$  is a good approximation of  $P$  if the computational error and the discretization error are both negligible compared with the modelling error  $P - \hat{A}_h$ . It is therefore critical to control the size of these two errors. Frequently, but not universally, it is possible to use Richardson extrapolation<sup>90,91</sup> to estimate the discretization error  $T - A_h$  by repeating the same simulation using different values of the time step  $h$ . In particular, Richardson extrapolation cannot be applied unless the force fields are sufficiently smooth<sup>90</sup>. Moreover, Richardson's error estimate is not reliable unless the computational error  $A_h - \hat{A}_h$  is sufficiently small<sup>90</sup>. The size of the computational error  $A_h - \hat{A}_h$  is controlled by the size of the unit roundoff  $u$  and the tolerance Tol that is passed to the constraint solver. In the absence of any information about the size of the discretization error  $T - A_h$ , the safest course of action is therefore to use the smallest practical value of the unit roundoff  $u$  and the tolerance Tol. This choice minimises the computational error and maximises the chance that the computational error is so small that we can reliably estimate the discretization error  $T - A_h$ . Therefore, it is prudent to favour double precision over single precision and tiny values of Tol over larger values of Tol. In ILVES we measure the relative constraint violation and iterate until

$$\frac{1}{2} \frac{\|r_{a_j} - r_{b_j}\|^2 - \sigma_j^2}{\sigma_j^2} \leq \text{Tol}$$

for all bonds or the maximum number of iterations is reached. If the relative constraint

violation is small, then

$$\frac{1}{2} \frac{\|r_{a_j} - r_{b_j}\|^2 - \sigma_j^2}{\sigma_j^2} = \frac{1}{2} \frac{(\|r_{a_j} - r_{b_j}\| - \sigma_j)(\|r_{a_j} - r_{b_j}\| + \sigma_j)}{\sigma_j^2} \approx \frac{\|r_{a_j} - r_{b_j}\| - \sigma_j}{\sigma_j}. \quad (23)$$

On a machine with unit roundoff  $u$  we cannot hope to reliably reduce the right-hand side below  $u$ . Therefore, the smallest value of Tol that should be considered is literally Tol =  $u$ .

## Complementary results

### Reliability calculations

We have calculated observable quantities to gauge whether their values change due to the usage of ILVES. The results of this analysis are summarized on Tab. S8, which presents the enthalpy change underwent upon the protein unfolding process ( $\Delta H_{unf}$ ), calculated as the difference between the average enthalpies of the simulated folded and unfolded states of the protein; the heat capacity change ( $\Delta C_{p_{unf}}$ ); and the Gibbs free energy ( $\Delta G_{unf}$ ) associated with this biological event<sup>82,83</sup>. Simulations were conducted on two extensively studied protein models, barnase and nuclease, applying two constraint tolerances,  $10^{-4}$  and  $10^{-10}$ , while keeping all other simulation parameters unchanged. Tab. S8 indicates that for ILVES and state-of-the-art solvers the evaluated thermodynamics  $\Delta H_{unf}(T_m)$  and  $\Delta G_{unf}(298K)$  fall within the error ranges defined by experimental measurements, for both proteins. In the case of  $\Delta C_{p_{unf}}$  the MD-calculated values fall outside the experimental ranges in some of the setups assessed, but the differences have similar sizes for all constraint solvers. This outcome supports the thesis that ILVES algorithms preserve system dynamics and do not introduce distortions larger than those due to traditionally employed constraint solvers.

Plots of the thermodynamics observables,  $\Delta H_{unf}$ ,  $\Delta C_{p_{unf}}$  and  $\Delta G_{unf}$ , computed from

Table S8: Experimentally measured and calculated (MD) thermodynamic quantities of unfolding ( $\Delta H_{unf}$  and  $\Delta C_{p_{unf}}$ ) for barnase ( $T_m = 323.0 \pm 0.7$  at pH  $\sim 4.1$ <sup>83</sup>) and nuclease ( $T_m = 326.9 \pm 0.4$  at pH  $\sim 7.0$ <sup>83</sup>). The listed Gibbs free energies ( $\Delta G_{unf}$ ) are calculated through the Gibbs-Helmholtz equation using either the measured or MD thermodynamics. The given errors are described above in the SI section “Observable quantities”. P-LINCS is configured with GROMACS default parameters, while MP-LINCS uses `lincs-order=4`.

Protein (Method)	Solver	Tol.	$\Delta H_{unf}$ at $T_m$ (kcal/mol)	$\Delta C_{p_{unf}}$ (kcal/mol · K)	$\Delta G_{unf}$ at 298 K (kcal/mol)
Barnase (Exp.)	—	—	$118.7 \pm 4.9$	$1.4 \pm 0.1$	$7.8 \pm 1.6$
Barnase (MD)	SHAKE	$10^{-4}$	$113.9 \pm 3.1$	$1.1 \pm 0.1$	$7.8 \pm 1.1$
	SHAKE	$10^{-10}$	$115.2 \pm 3.1$	$1.3 \pm 0.1$	$7.6 \pm 1.4$
	MP-LINCS	$10^{-4}$	$116.9 \pm 3.1$	$1.2 \pm 0.0$	$7.9 \pm 1.2$
	MP-LINCS	$10^{-10}$	$118.6 \pm 3.1$	$1.3 \pm 0.1$	$7.9 \pm 1.3$
	P-LINCS	—	$116.3 \pm 3.1$	$1.2 \pm 0.0$	$7.9 \pm 1.2$
	ILVES-M	$10^{-4}$	$113.6 \pm 3.1$	$1.0 \pm 0.1$	$7.8 \pm 1.2$
	ILVES-M	$10^{-10}$	$117.4 \pm 3.1$	$1.1 \pm 0.2$	$8.0 \pm 1.3$
	ILVES-F	$10^{-4}$	$116.4 \pm 3.1$	$1.2 \pm 0.0$	$7.8 \pm 1.2$
	ILVES-F	$10^{-10}$	$115.6 \pm 3.1$	$1.0 \pm 0.1$	$7.9 \pm 1.2$
Nuclease (Exp.)	—	—	$82.1 \pm 4.7$	$2.3 \pm 0.1$	$4.2 \pm 1.6$
Nuclease (MD)	SHAKE	$10^{-4}$	$78.1 \pm 4.8$	$2.0 \pm 0.1$	$4.2 \pm 1.4$
	SHAKE	$10^{-10}$	$73.5 \pm 4.8$	$1.9 \pm 0.1$	$4.1 \pm 1.3$
	MP-LINCS	$10^{-4}$	$74.6 \pm 4.8$	$1.8 \pm 0.1$	$4.2 \pm 1.3$
	MP-LINCS	$10^{-10}$	$71.6 \pm 4.8$	$1.7 \pm 0.2$	$4.1 \pm 1.4$
	P-LINCS	—	$70.8 \pm 4.8$	$1.6 \pm 0.0$	$4.2 \pm 1.1$
	ILVES-M	$10^{-4}$	$75.8 \pm 4.8$	$2.0 \pm 0.1$	$4.0 \pm 1.4$
	ILVES-M	$10^{-10}$	$74.6 \pm 4.8$	$2.0 \pm 0.1$	$4.0 \pm 1.4$
	ILVES-F	$10^{-4}$	$74.4 \pm 4.8$	$2.0 \pm 0.0$	$4.0 \pm 1.3$
	ILVES-F	$10^{-10}$	$73.1 \pm 4.8$	$1.8 \pm 0.1$	$4.1 \pm 1.3$



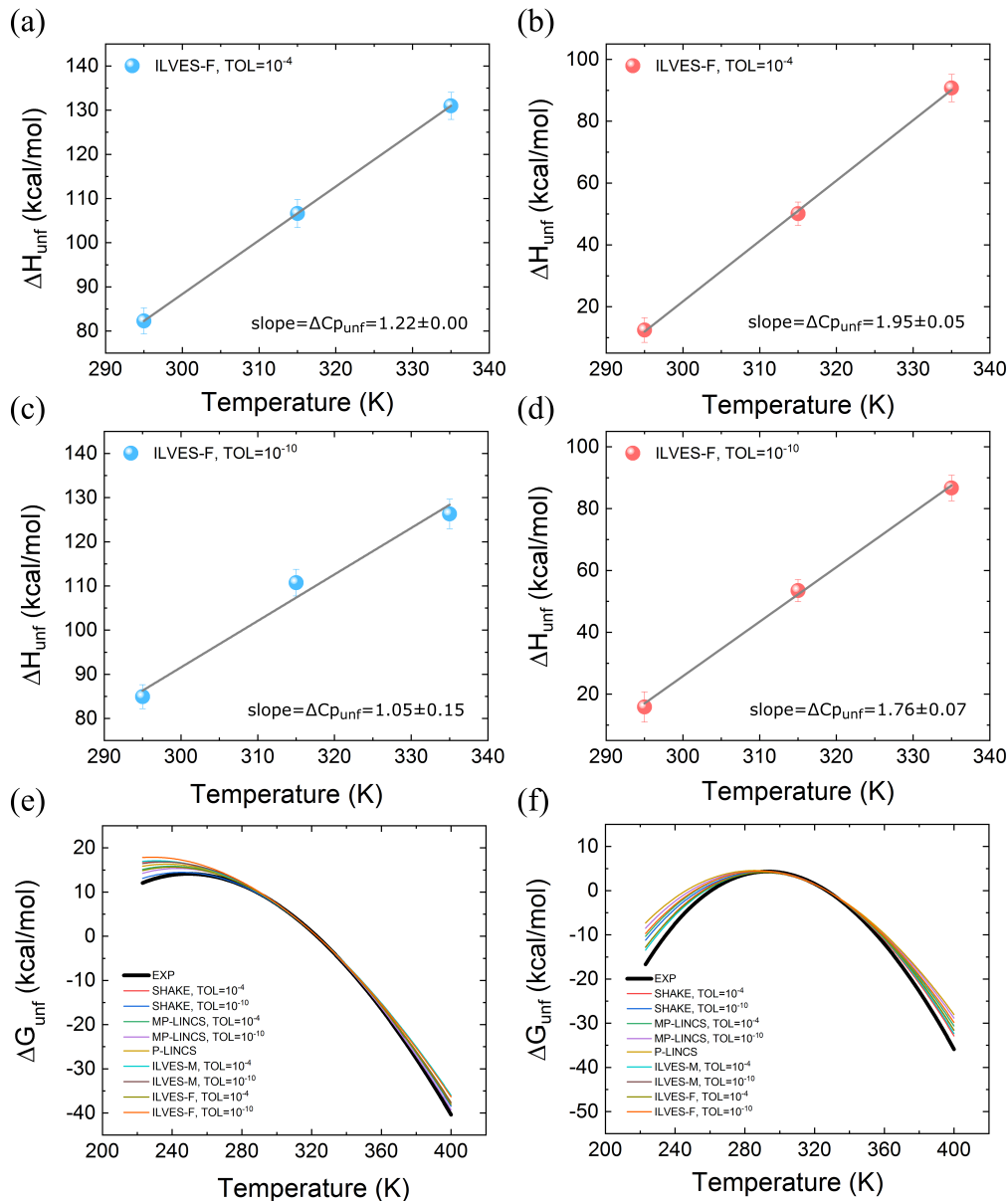


Figure S8: Observable quantities obtained from experimental measurements compared to the corresponding computed quantities from simulations with our ILVES algorithms and the state-of-the-art constraint solvers. (a and b) Enthalpy change of unfolding plotted versus temperature for barnase and nuclease, respectively, simulated with ILVES-F at the constraint tolerance of  $10^{-4}$ . (c and d) Enthalpy change of unfolding plotted versus temperature for barnase and nuclease, respectively, simulated with ILVES-F at the constraint tolerance of  $10^{-10}$ . The slope of the linear relationships shown represents the  $\Delta C_{p_{unf}}$  of the process. These plots (a-d) are shown as an example of all the plots obtained for the different constraint solvers evaluated.

the simulations accomplished, are given in Fig. S8. For the sake of proper comparison, in the case of  $\Delta G_{unf}$ , the calculated Gibbs free-energy profiles of the proteins are plotted along with the corresponding experimental profiles. Errors associated with the experimental values reported in the Tab. of the main paper are those given in Ref.<sup>83</sup>, which were calculated as the standard error of the mean of a number of measurements reported by several groups.

Our results indicate that for ILVES and state-of-the-art solvers, the evaluated thermodynamics  $\Delta H_{unf}(T_m)$  and  $\Delta G_{unf}(298K)$  fall within the error ranges defined by experimental measurements, for both proteins. In the case of  $\Delta C_{p_{unf}}$ , the MD-calculated values fall outside the experimental ranges in some of the setups assessed, but the differences have similar sizes for all constraint solvers. This outcome supports the thesis that ILVES algorithms preserve system dynamics and do not introduce distortions larger than those due to traditionally employed constraint solvers.

## Further discussion about the performance

In this section, we extend and provide more detail to the performance results presented in the main paper.

The time spent in the initialization of the solvers can be high in distributed memory simulations. For this reason, the execution times in our analysis include both initialization and processing for all solvers except ILVES-PC. This solver, released as a proof of concept without distributed memory support, did not include an optimized initialization.

Constraining only H-bonds is the most usual way to proceed, though imposing constraints on all bond lengths is also a common practice. The latter is recommended in terms of physical reliability<sup>6</sup> because these degrees of freedom are better described by *quantum* harmonic oscillators<sup>35</sup> than by classical harmonic oscillators, since vibrational frequencies of bonds are over 10 times higher than  $k_B T / \hbar$  at room temperature<sup>4,92</sup>. Moreover, the dynamics are not significantly affected by imposing constraints on all bonds; for example, the average

values of bond and dihedral angles are hardly affected by bond length constraints<sup>93</sup>. On the other hand, constraining H-angles has been rather uncommon to date. It is most likely that this is at least partly due to the fact that none of the commonly used constraint algorithms (SHAKE and P-LINCS, which are the options offered by GROMACS) can deal with coupled angle constraints satisfactorily: P-LINCS often crashes<sup>14</sup> while GROMACS' sequential implementation of SHAKE converges very slowly<sup>16</sup>.

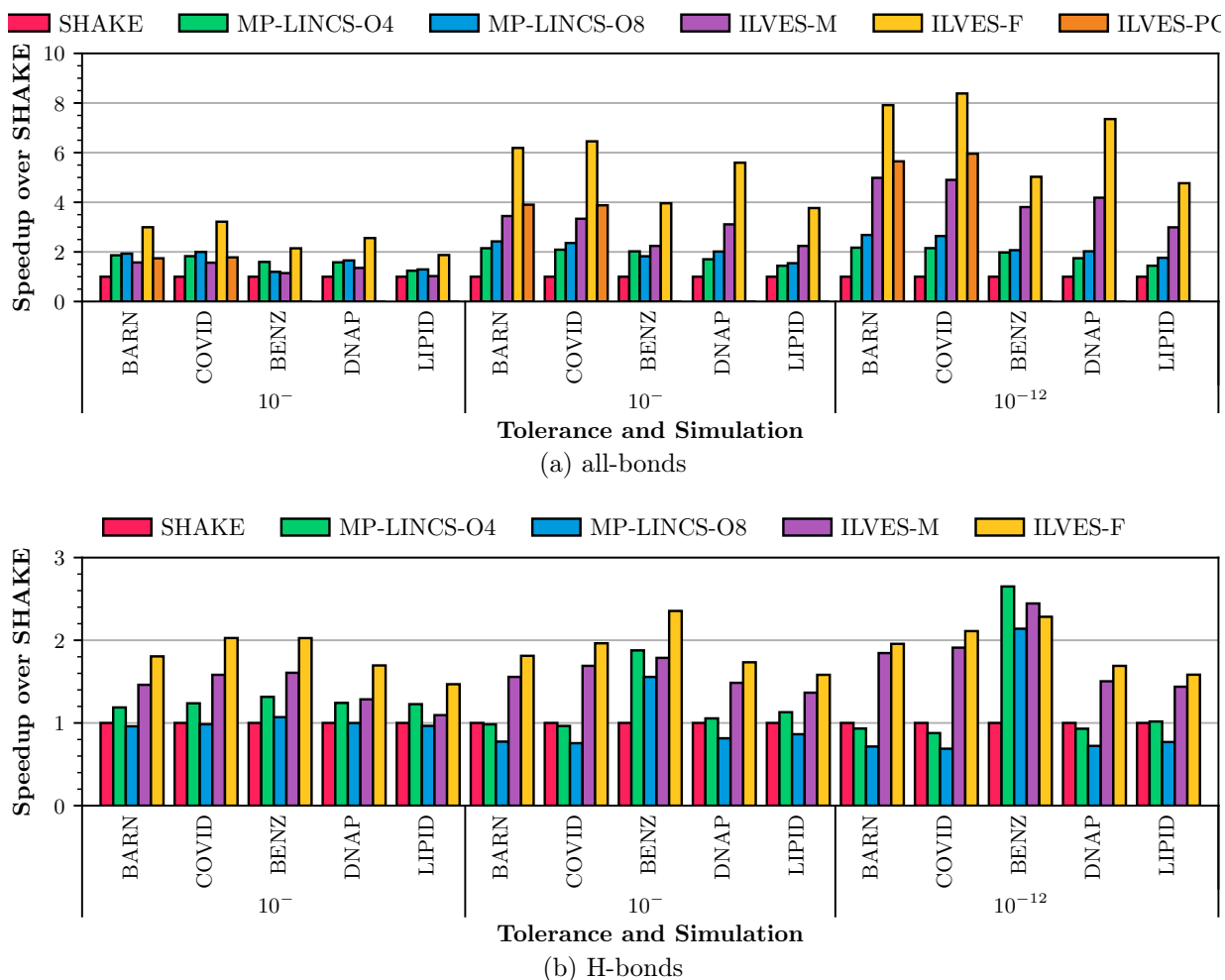


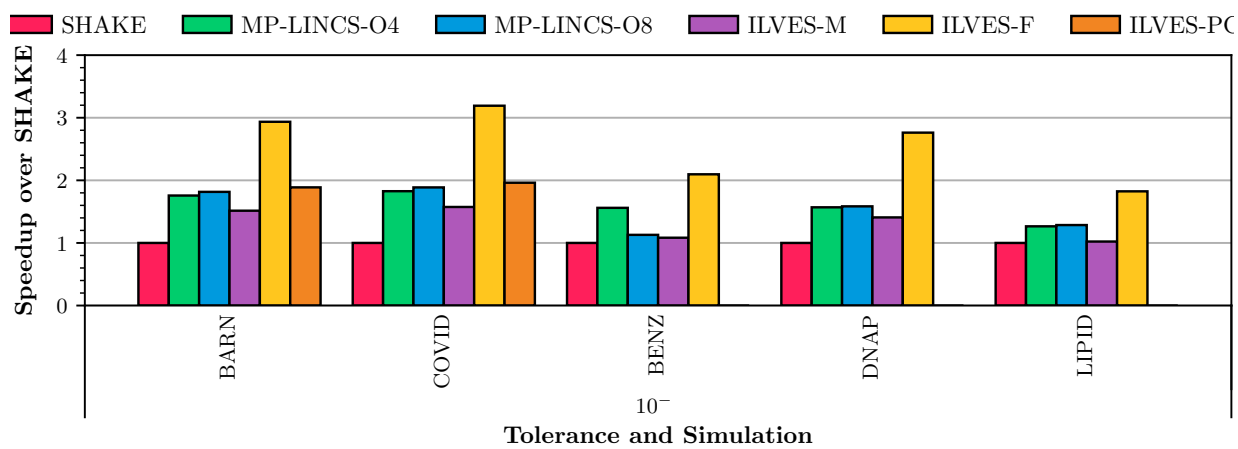
Figure S9: Single-thread speedup over SHAKE of MP-LINCS (lincs-order=4 and lincs-order=8), ILVES, ILVES-F and ILVES-PC.

Fig. S9 displays the *single-thread* speedup over SHAKE. While ILVES-PC is tailored to protein simulations, it delivers only modest speedups over ILVES-M, which incorporates optimizations absent in ILVES-PC, the most significant being the vectorization of linear-system

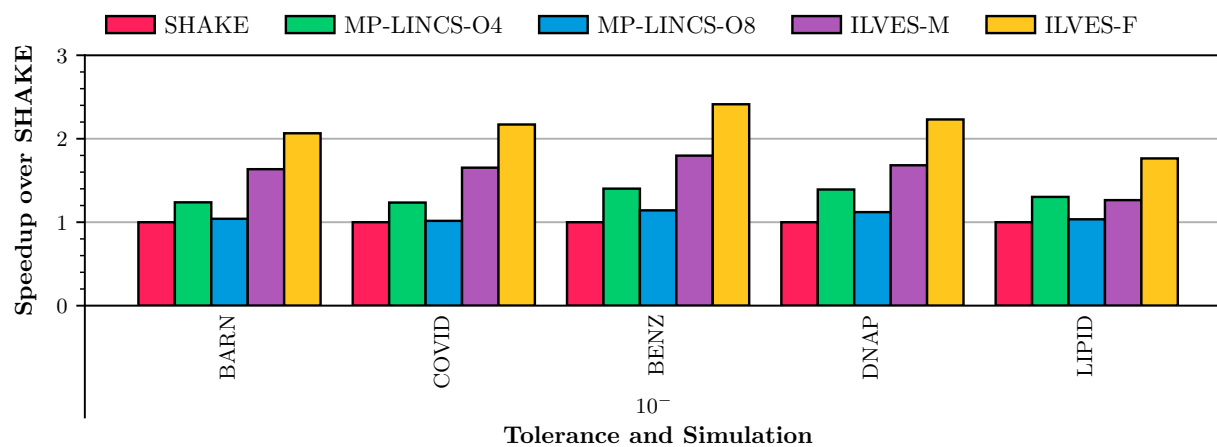
construction. When constraining all-bonds and using  $\text{Tol} = 10^{-4}$ , ILVES-M and ILVES-PC achieve speedups between  $1\times$  and  $1.8\times$  compared to SHAKE, similar to MP-LINCS. For the same tolerance, ILVES-F outperforms both, delivering speedups between  $1.9\times$  and  $3.2\times$  over SHAKE and between  $1.5\times$  and  $1.8\times$  over MP-LINCS. As the tolerance becomes more demanding, all ILVES versions show greater speedups, with a maximum of  $8.4\times$  over SHAKE and  $4.2\times$  over MP-LINCS. For `constraints=h-bonds`, MP-LINCS performs similarly to SHAKE in most simulations, while ILVES-M and ILVES-F show consistent speedups over both SHAKE and MP-LINCS across all tolerances, achieving maximum speedups of  $2.4\times$  and  $3\times$  over SHAKE and MP-LINCS, respectively. The only case on Fig. S9 where MP-LINCS outperforms ILVES-F is the BENZ simulation at the tightest tolerance. In it each benzene molecule has only six constraints, and MP-LINCS achieves low errors in its projection step, sometimes avoiding any iteration of its correction step. Note that the benzene molecule with constraints on just H-bonds is a very exceptional case where every constraint is fully decoupled from the rest. This makes the matrix which must be inverted in the involved linear systems of equations ( $\mathbf{A}$ ) be diagonal because there exists no atom which belongs to two different constraints, which makes the linear system to be suitable for a faster analytical solution. Relevant research works recommend to constrain both bond lengths and bond angles in benzene<sup>41</sup>.

Figs. S10, S11, and S12 present the single-precision counterparts of the double-precision results shown previously or in the main paper. In single-precision, tolerances of  $10^{-8}$  and  $10^{-12}$  are not achievable; therefore, only  $\text{Tol}=10^{-4}$  is reported. These figures can be directly compared to the  $\text{Tol}=10^{-4}$  results in double-precision, showing that single-precision execution does not impact the comparison between solvers. The single-precision comparison at  $\text{Tol}=10^{-4}$  is nearly identical to that in double-precision.

In the analysis provided in the main text, we display results of efficiency for a given tolerance in satisfying the constraints, which is an input parameter of the simulation. Nevertheless, one should not confuse such tolerance with the actual accuracy in satisfying the



(a) All bonds



(b) H-bonds

Figure S10: Single-thread speedup over SHAKE of MP-LINCS (lincs-order=4 and lincs-order=8), ILVES-M, ILVES-F and ILVES-PC for calculations in single precision arithmetic. (a) Constraints imposed on all bonds; (b) On H-bonds.

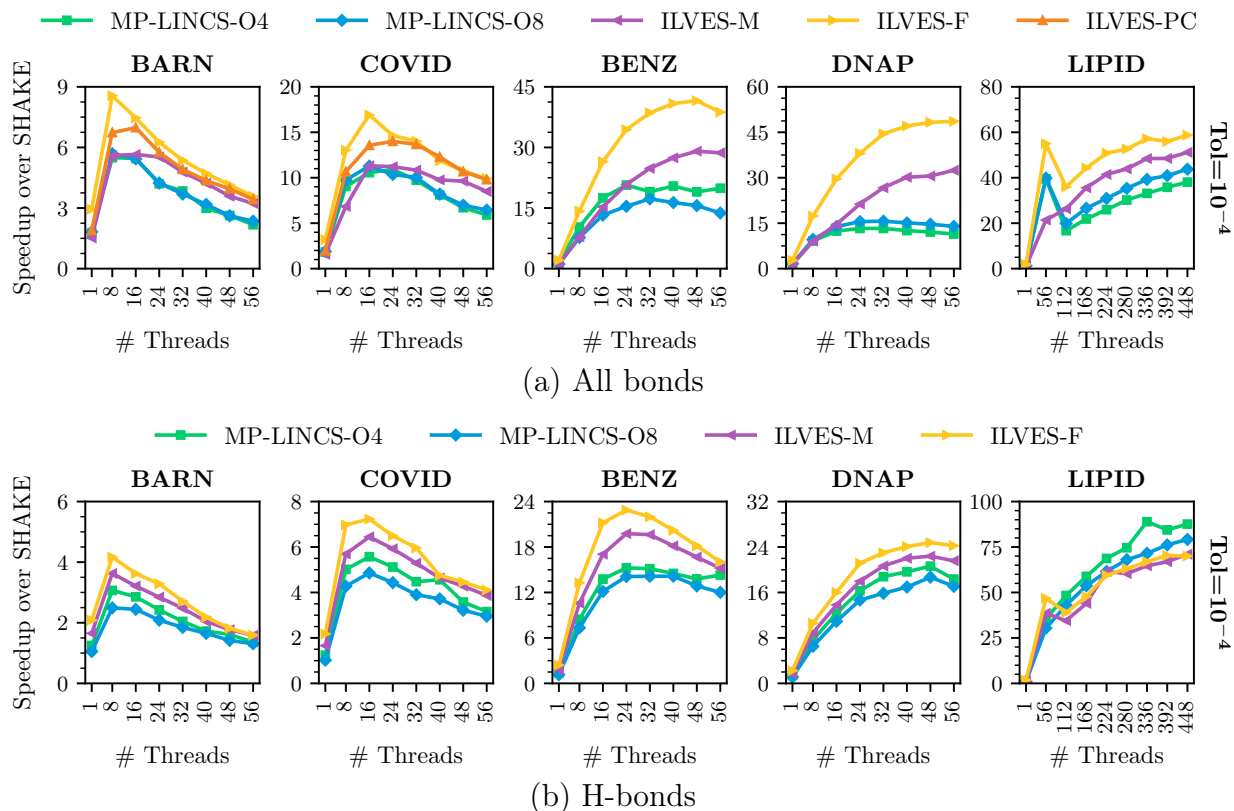


Figure S11: Single-precision multi-thread speedup over SHAKE of MP-LINCS (`lincs-order=4` and `lincs-order=8`), ILVES-M, ILVES-F and ILVES-PC. The BARN, COVID, BENZ and DNAP simulations are executed using a single task in a single chip of a computing node. The LIPID simulation is executed using up to 8 tasks (up to 4 nodes and 8 chips). (a) Constraints imposed on all bonds; (b) On H-bonds.

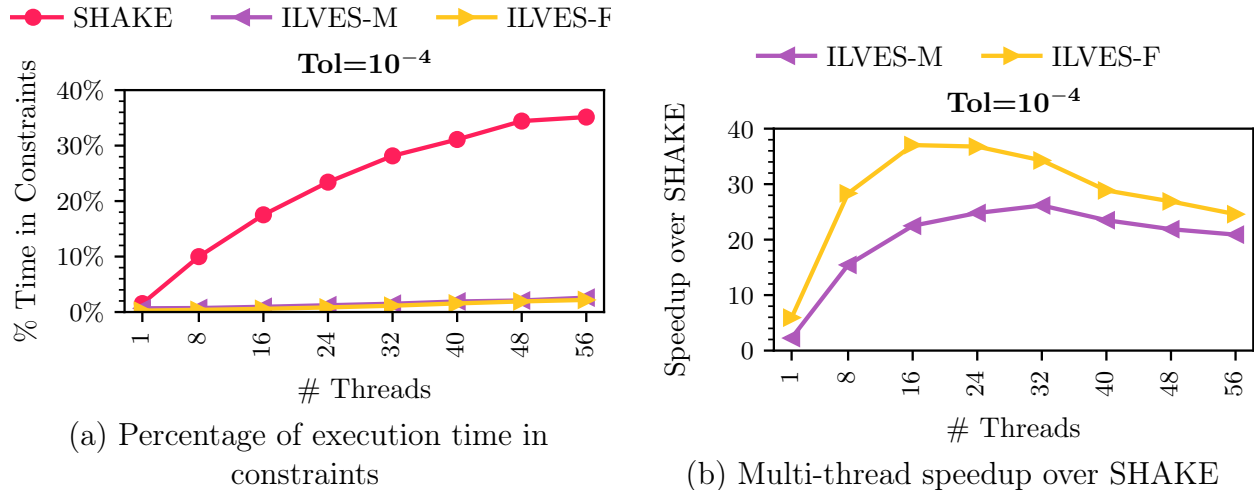
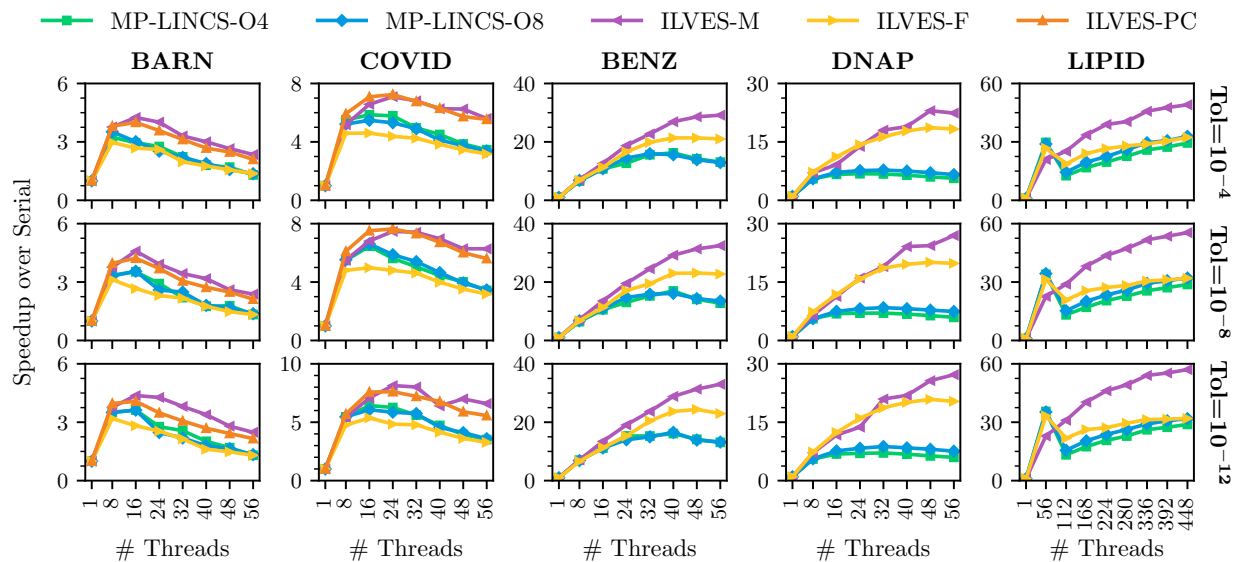


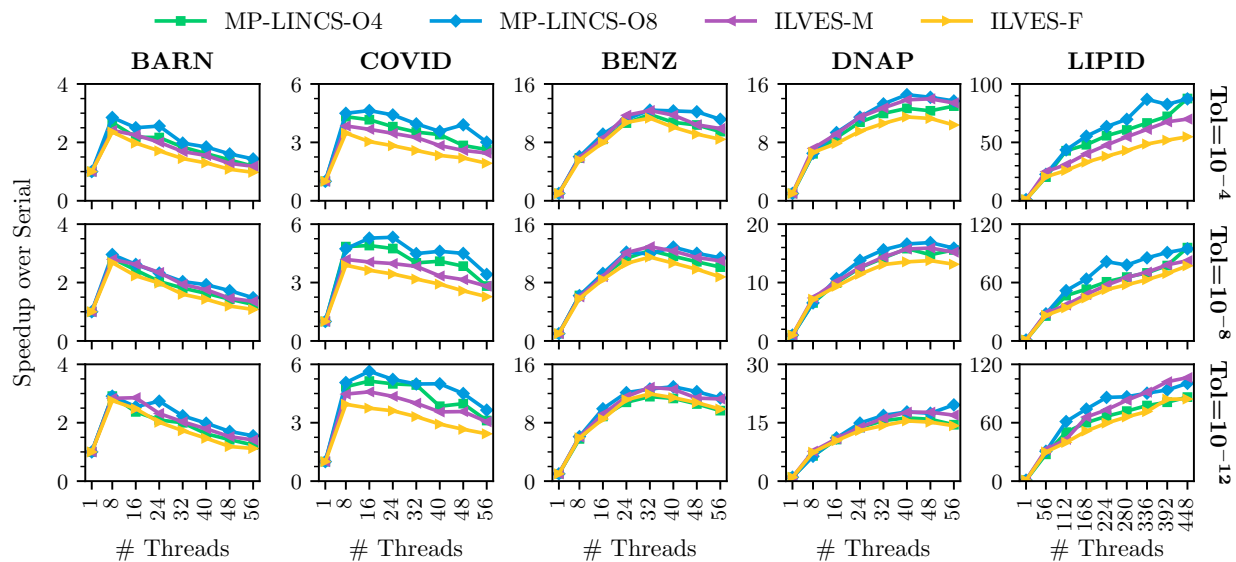
Figure S12: Results of SHAKE, ILVES-M and ILVES-F in the COVID main protease simulation imposing constraints on all bonds and H-angles with different tolerances. (a) Percentage of the total execution time taken by SHAKE, ILVES-M, and ILVES-F; (b) Multi-thread speedup of ILVES-M and ILVES-F with respect to SHAKE.

constraints: the average relative error in satisfying the constraints can be either slightly lower than the tolerance or much lower than it. Despite the fact that tolerance defines the maximum acceptable error, the rapid convergence of the ILVES algorithms often yields errors significantly below this threshold. This results in accuracy gains, providing a compelling reason to choose ILVES over (M)P-LINCS in simulations where their performance is similar. To illustrate this, we measured the average relative error achieved by ILVES and MP-LINCS in the BENZ and LIPID simulations with  $\text{Tol} = 10^{-4}$  and **constraints=h-bonds**. In the BENZ simulation, MP-LINCS-O4 and MP-LINCS-O8 achieve average relative errors of  $8.6 \times 10^{-6}$  and  $1.3 \times 10^{-6}$ , respectively, while ILVES-M and ILVES-F achieve average relative errors of  $7 \times 10^{-11}$  and  $9.6 \times 10^{-8}$ , respectively. Similarly, in the LIPID simulation, MP-LINCS-O4 and MP-LINCS-O8 achieve average relative errors of  $6.6 \times 10^{-7}$  and  $1.9 \times 10^{-6}$ , respectively, while ILVES-M and ILVES-F achieve average relative errors of  $4.7 \times 10^{-10}$  and  $1.7 \times 10^{-7}$ , respectively. Note that LIPID with  $\text{Tol} = 10^{-4}$  is the only case presented in the main text where MP-LINCS' delivers better speedup over SHAKE than ILVES'; however, ILVES provides enhanced accuracy at the cost of very low additional computing time.

Figs. S13 and S14 illustrate the speedup achieved by the parallel solvers relative to serial



(a) All bonds



(b) H-bonds

Figure S13: Multi-thread speedup over serial execution of MP-LINCS (`lincs-order=4` and `lincs-order=8`), ILVES-M, ILVES-F and ILVES-PC. The BARN, COVID, BENZ and DNAP simulations are executed using a single task in a single chip of a computing node. The LIPID simulation is executed using up to 8 tasks (up to 4 nodes and 8 chips). Calculations performed in double precision arithmetic. (a) Constraints imposed on all bonds; (b) On H-bonds.



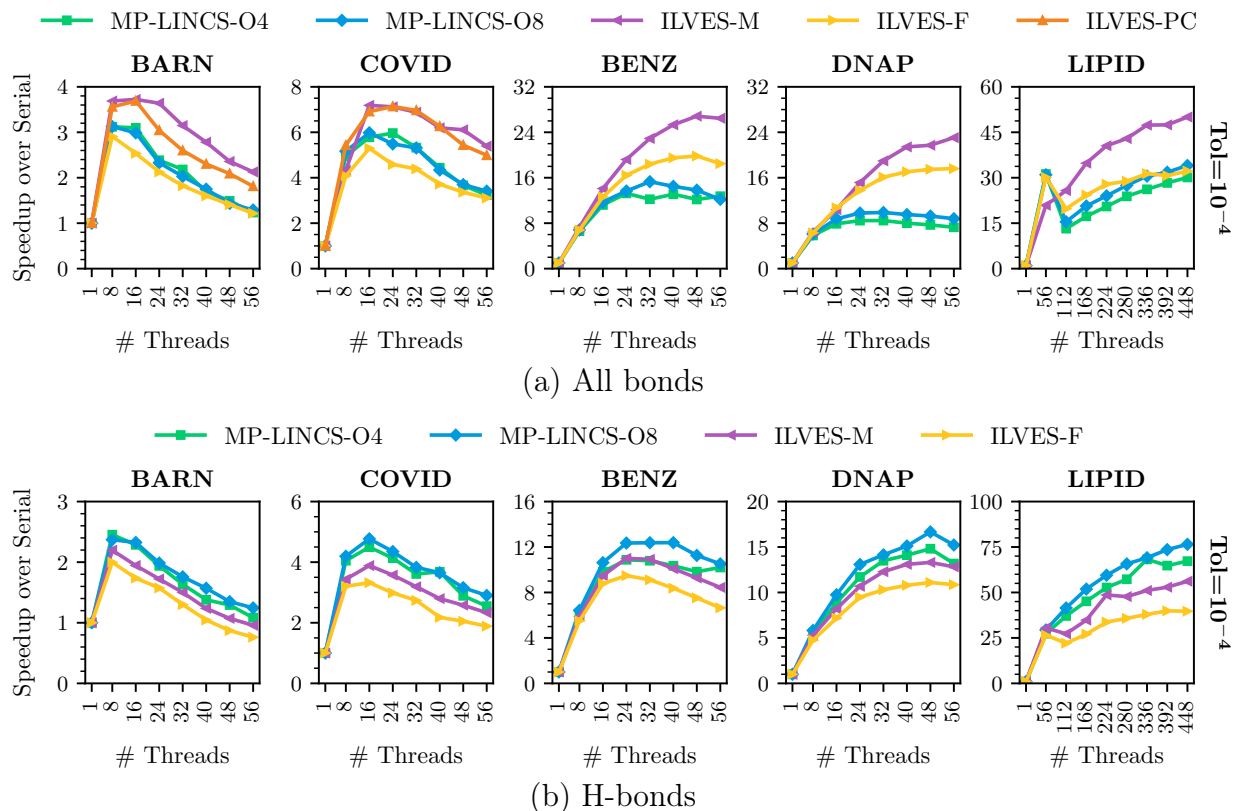
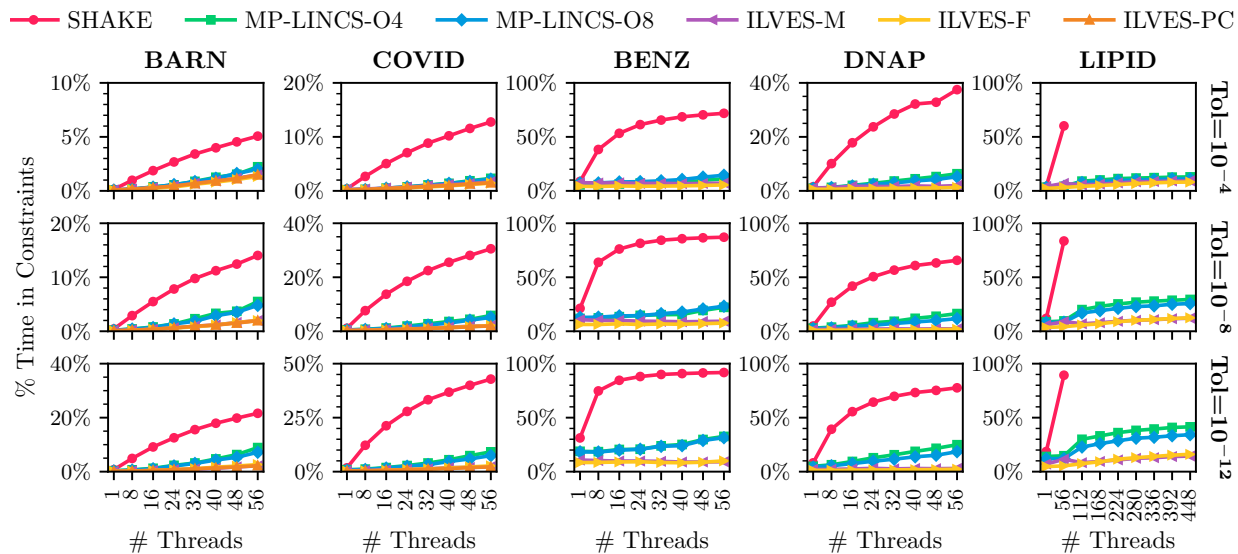


Figure S14: Single-precision multi-thread speedup over serial execution of MP-LINCS (`lincs-order=4` and `lincs-order=8`), ILVES-M, ILVES-F and ILVES-PC. The BARN, COVID, BENZ and DNAP simulations are executed using a single task in a single chip of a computing node. The LIPID simulation is executed using up to 8 tasks (up to 4 nodes and 8 chips). (a) Constraints imposed on all bonds; (b) On H-bonds.

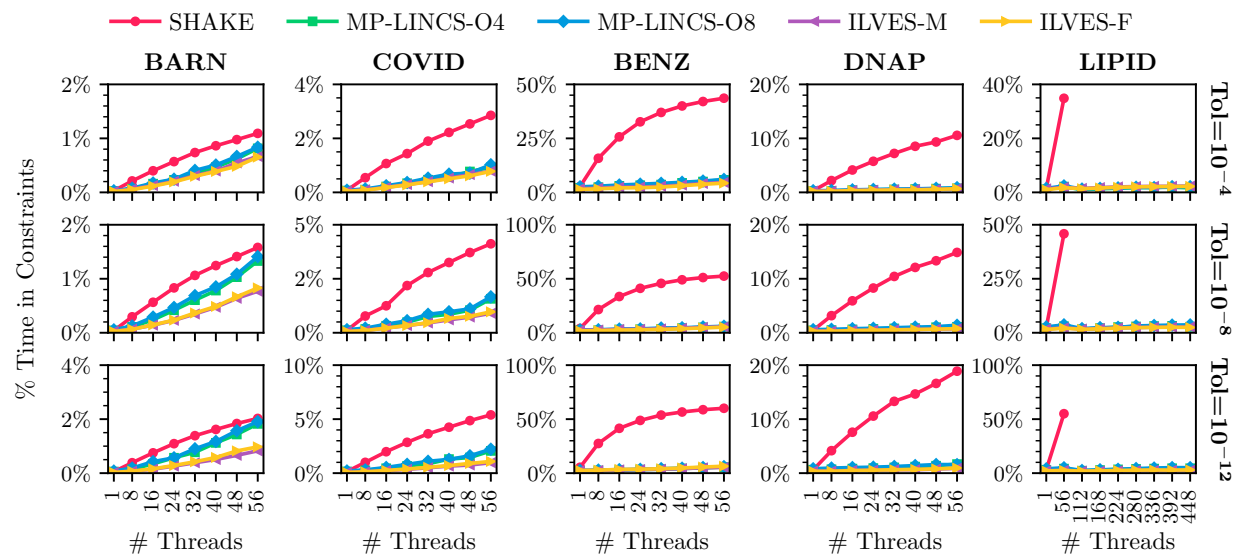
execution. The scalability of a solver is defined as the ratio of the execution time of the solver using  $N$  threads to the execution time of the solver using 1 thread. As noted earlier, the single-precision results are comparable to the double-precision results with  $\text{Tol}=10^{-4}$ . The parallel scalability of the new ILVES algorithms is significantly better in the BENZ and DNAP simulations with `constraints=all-bonds`. In these simulations, the graph partitioning produced by ILVES-M results in substantially less serial work compared to MP-LINCS. In the case of BENZ, the partitioning eliminates serial work entirely. While in other simulations the scalability of the ILVES algorithms and MP-LINCS is more similar, it is important to note that ILVES delivers better performance than MP-LINCS in most cases. Consequently, for shorter execution times, the overhead of thread synchronization in ILVES becomes more pronounced, ultimately affecting its parallel scalability.

In most parallel simulations peak performance is not achieved using the maximum number of threads available. As more threads are added, synchronization overhead increases, and if zero-cut partitions are not possible, the amount of serial code executed also rises. When the parallel work becomes insufficient to offset the synchronization cost and serial execution the performance begins to decline. This behaviour is particularly evident in the lipid bilayer simulation with `constraints=all-bonds`, where a performance drop occurs beyond 56 threads. This decline corresponds to the transition from a single task to multiple tasks, which increases synchronization and serial execution. In contrast, this drop is absent with `constraints=h-bonds` due to the lack of bonds between atoms in different tasks, thereby eliminating the need for inter-task communication.

Figs. S15 and S16 display the percentage of the total simulation execution time spent in the constraint solver (excluding water). In our multi-threaded simulations, with `constraints=all-bonds`, SHAKE accounts for up to 92% of the total execution time, MP-LINCS up to 42%, and ILVES up to 16%. With `constraints=h-bonds`, SHAKE accounts for up to 60%, MP-LINCS up to 6%, and ILVES up to 5%.

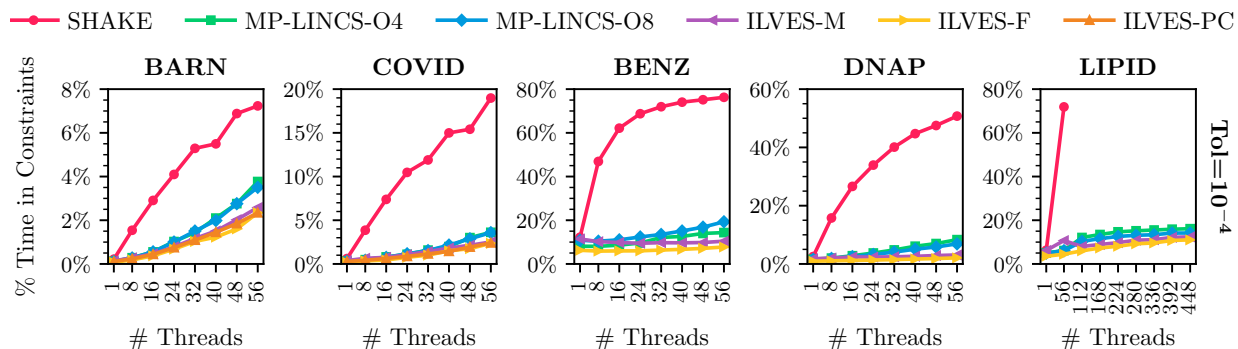


(a) All bonds

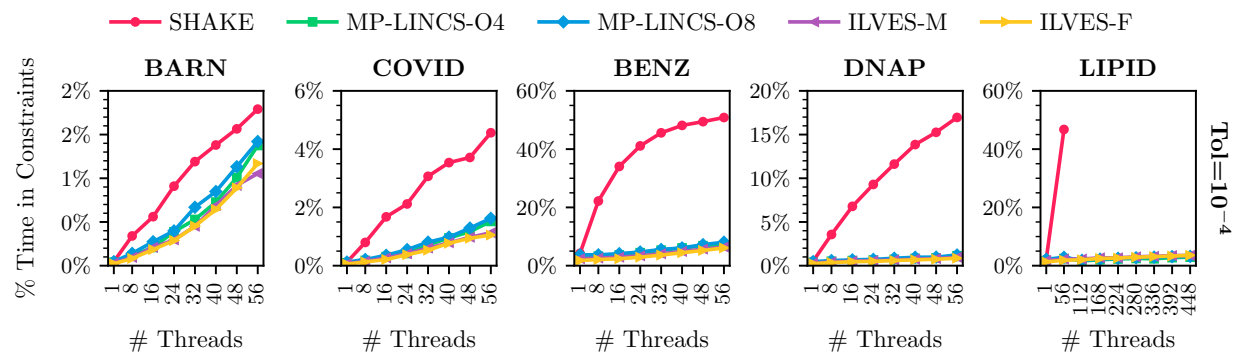


(b) H-bonds

Figure S15: Double-precision percentage of the total execution time of **Gromacs** spent in the constraint solver (ex water). (a) constraints imposed on all bonds; (b) On H-bonds.



(a) All bonds



(b) H-bonds

Figure S16: Single-precision percentage of the total execution time of **Gromacs** spent in the constraint solver (ex water). (a) constraints imposed on all bonds; (b) On H-bonds.

## Future research

The continuation of our research will mainly consist of two areas: further optimization of the code and extension of the scope of the algorithm. The optimization will rely on both algorithmic and implementation improvements. Among the former, we highlight successive over-relaxation methods which have been successful with SHAKE<sup>11</sup>, though we will also analyse other works<sup>94</sup>; we also consider speeding up the calculations through an appropriate starting guess ( $\lambda_{k,0} \neq \mathbf{0}$ ) obtained with machine learning using atomic coordinates as input. Concerning implementation improvements, we plan to make compiled (loop-free) code to be automatically generated for every arbitrary simulated molecule. In addition, we will apply vectorization whenever possible. Moreover, we aim to generate a GPU version of ILVES for handling constraints, following the approach of P-LINCS. In the past we applied vectorization and loop-free code in solving the constraints of small molecules, obtaining nice efficiency enhancements<sup>88</sup>. Preliminary analysis indicates that optimization of ILVES through vectorization could solve constraints on water molecules very fast, and hence make it an alternative to the celebrated SETTLE algorithm<sup>20</sup>. The usage of a single constraint solver for all molecules within a given simulation would make the simulation simpler, avoiding possible inconsistencies. We will also consider implementing ILVES-L, a further member of the ILVES family, which solves LINCS' equations rather than SHAKE's.

Concerning the extension of the scope of the algorithm, we plan to develop code which is capable of constraining bond angles of heavy atoms (not necessarily through distance constraints<sup>35</sup>) as well as dihedral angles<sup>36</sup>. In this line we plan to deeply analyse how imposing such constraints affects the dynamics of the simulated molecules. The calculation of the corresponding Lagrange multipliers is expected to remain fast because ILVES is based on direct solvers and because the topology of biological molecules frequently causes the coordinate matrix of the linear systems of equations to solve be banded<sup>86,87</sup>, which reduces the number of fillings. We deem this line very promising because constraining internal degrees of freedom other than bond lengths and H-angles would enable one to further

increase the time step of the simulations<sup>3,6</sup> thus making it possible to simulate a wider set of phenomena.

## References

- (1) Ryckaert, J. P.; Ciccotti, G.; Berendsen, H. J. C. Numerical integration of the Cartesian equations of motion of a system with constraints: Molecular dynamics of n-alkanes. *J. Comput. Phys.* **1977**, *23*, 327–341.
- (2) Hess, B. P-LINCS: A parallel linear constraint solver for molecular simulation. *J. Chem. Theory Comput.* **2008**, *4*, 116–122.
- (3) Mazur, A. Hierarchy of Fast Motions in Protein Dynamics. *J. Phys. Chem. B* **1998**, *102*, 473–479.
- (4) van Gunsteren, W. F.; Bonvin, A. M.; Daura, X.; Smith, L. J. Aspects of modeling biomolecular structure on the basis of spectroscopic or diffraction data. *Biological Magnetic Resonance: Structure Computation and Dynamics in Protein NMR* **2002**, 3–35.
- (5) Feenstra, K. A.; Hess, B.; Berendsen, H. J. C. Improving efficiency of large time-scale molecular dynamics simulations of hydrogen-rich Systems. *J. Comput. Chem.* **1999**, *20*, 786–798.
- (6) Stocker, U.; Juchli, D.; van Gunsteren, W. F. Increasing the time step and efficiency of molecular dynamics simulations: optimal solutions for equilibrium simulations or structure refinement of large biomolecules. *Molecular Simulation* **2003**, *29*, 123–138.
- (7) Pechlaner, M.; van Gunsteren, W. F. On the use of intra-molecular distance and angle

- constraints to lengthen the time step in molecular and stochastic dynamics simulations of proteins. *Proteins: Structure, Function, and Bioinformatics* **2022**, *90*, 543–559.
- (8) Inada, Y.; Loeffler, H. H.; Rode, B. M. Librational, vibrational, and exchange motions of water molecules in aqueous Ni (II) solution: classical and QM/MM molecular dynamics simulations. *Chem. Phys. Lett.* **2002**, *358*, 449–458.
  - (9) Verlet, L. Computer "experiments" on classical fluids. I. Thermodynamical properties of Lennard-Jones molecules. *Phys. Rev.* **1967**, *159*, 98–103.
  - (10) Hairer, E.; Wanner, G.; Lubich, C. *Geometric Numerical Integration*; Springer, 2006.
  - (11) Barth, E.; Kuczera, K.; Leimkuhler, B.; Skeel, R. D. Algorithms for constrained Molecular Dynamics. *J. Comput. Phys.* **1995**, *16* (10), 1192–1209.
  - (12) López-Villellas, L.; Mikkelsen, C.; Galano, J.; Marco-Sola, S.; Alastruey, J.; Ibáñez Marín, P.; Moretó, M.; Sancho, J.; García-Risueño, P. Accurate and efficient constrained molecular dynamics of polymers using Newton's method and special purpose code. *Computer Physics Communications* **2023**, *288*, 108742.
  - (13) Hess, B.; Bekker, H.; Berendsen, H. J. C.; Fraaije, J. G. E. M. LINCS: A Linear constraint solver for molecular simulations. *J. Comput. Chem.* **1997**, *18*, 1463–1472.
  - (14) Broadbent, R. J.; Spencer, J. S.; Mostofi, A. A.; Sutton, A. P. Accelerated simulations of aromatic polymers: application to polyether ether ketone (PEEK). *Molecular Physics* **2014**, *112*, 2672–2680.
  - (15) van Gunsteren, W. F.; Daura, X.; Fuchs, P. F.; Hansen, N.; Horta, B. A.; Hünenberger, P. H.; Mark, A. E.; Pechlaner, M.; Riniker, S.; Oostenbrink, C. On the effect of the various assumptions and approximations used in molecular simulations on the properties of bio-molecular systems: overview and perspective on issues. *ChemPhysChem* **2021**, *22*, 264–282.

- (16) Wacha, A.; Varga, Z.; Beke-Somfai, T. Comparative Study of Molecular Mechanics Force Fields for  $\beta$ -Peptidic Foldamers: Folding and Self-Association. *Journal of Chemical Information and Modeling* **2023**, *63*, 3799–3813.
- (17) Moré, J. J. Nonlinear Generalizations of Matrix Diagonal Dominance with Application to Gauss–Seidel Iterations. *SIAM Journal on Numerical Analysis* **1972**, *9*, 357–378.
- (18) Tao, P.; Wu, X.; Brooks, B. R. Maintain rigid structures in Verlet based Cartesian molecular dynamics simulations. *J. Chem. Phys.* **2012**, *137*.
- (19) Andersen, H. C. Rattle: A “velocity” version of the SHAKE algorithm for Molecular Dynamics calculations. *J. Comput. Phys.* **1983**, *52*, 24–34.
- (20) Miyamoto, S.; Kollman, P. A. Settle: An analytical version of the SHAKE and RATTLE algorithm for rigid water models. *J. Comput. Chem.* **1992**, *13*, 952–962.
- (21) Lambrakos, S. G.; Boris, J.; Oran, E.; Chandrasekhar, I.; Nagumo, M. A modified SHAKE algorithm for maintaining rigid bonds in molecular dynamics simulations of large molecules. *J. Comput. Phys.* **1989**, *85*, 473–486.
- (22) Lee, S.-H.; Palmo, K.; Krimm, S. WIGGLE: A new constrained molecular dynamics algorithm in Cartesian coordinates. *J. Comput. Phys.* **2005**, *210*, 171–182.
- (23) Gonnet, P. P-SHAKE: a quadratically convergent SHAKE in  $O(n^2)$ . *J. Chem. Phys.* **2006**, *220*, 740–750.
- (24) Ciccotti, G.; Ryckaert, J.-P. Molecular dynamics simulation of rigid molecules. *Computer Physics Reports* **1986**, *4*, 346–392.
- (25) Ryckaert, J.-P.; Ariedi, G.; Melchionna, S. Molecular dynamics of polymers with explicit but frozen hydrogens. *Molecular Physics* **2001**, *99*, 155–165.



- (26) Eastman, P.; Pande, V. S. Constant Constraint Matrix Approximation: A robust, parallelizable constraint method for molecular simulations. *J. Chem. Theory Comput.* **2010**, *6*, 434–437.
- (27) Krautler, V.; Van Gunsteren, W. F.; Hunenberger, P. H. A fast SHAKE Algorithm to Solve Distance Constraint Equations for Small Molecules in Molecular Dynamics Simulations. *J. Comput. Chem.* **2001**, *22*, 501–508.
- (28) Christen, M.; van Gunsteren, W. F. An approximate but fast method to impose flexible distance constraints in molecular dynamics simulations. *J. Chem. Phys.* **2005**, *122*.
- (29) Bailey, A. G.; Lowe, C. P.; Sutton, A. P. Efficient constraint dynamics using MILC SHAKE. *J. Comput. Phys.* **2008**, *227*, 8949–8959.
- (30) Bailey, A. G.; Lowe, C. P. MILCH SHAKE: An efficient method for constraint dynamics applied to alkanes. *J. Comput. Chem.* **2009**, *30*, 2485–2493.
- (31) Mazars, M. Holonomic constraints, an analytical result. *J. Phys. A: Math. Theor.* **2007**, *49*, 1747–1755.
- (32) Weinbach, Y.; Elber, R. Revisiting and parallelizing SHAKE. *J. Comput. Phys.* **2005**, *209*, 193–206.
- (33) Elber, R.; Ruymgaart, A.; Hess, B. SHAKE parallelization. *Eur. Phys. J. Spec. Top.* **2011**, *200*, 211–223.
- (34) Gonnet, P.; Walther, J. H.; Koumoutsakos, P. Theta SHAKE: An extension to SHAKE for the explicit treatment of angular constraints. *Comput. Phys. Comm.* **2009**, *180*, 360–364.
- (35) Pechlaner, M.; Dorta, A. P.; Lin, Z.; Rusu, V. H.; van Gunsteren, W. F. A method to apply bond-angle constraints in molecular dynamics simulations. *J. Comput. Chem.* **2021**, *42*, 418–434.

- (36) Pechlaner, M.; van Gunsteren, W. F. Algorithms to apply dihedral-angle constraints in molecular or stochastic dynamics simulations. *J. Chem. Phys* **2020**, *152*.
- (37) Dubbeldam, D.; Oxford, G. A.; Krishna, R.; Broadbelt, L. J.; Snurr, R. Q. Distance and angular holonomic constraints in molecular simulations. *The Journal of chemical physics* **2010**, *133*.
- (38) Hayashi, Y.; Shiomi, J.; Morikawa, J.; Yoshida, R. RadonPy: automated physical property calculation using all-atom classical molecular dynamics simulations for polymer informatics. *npj Computational Materials* **2022**, *8*, 222.
- (39) Huda, M. M.; Rai, N. Probing early-stage aggregation of low molecular weight gelator in an organic solvent. *J. Phys. Chem. B* **2020**, *124*, 2277–2288.
- (40) Ciulla, M. G.; Fontana, F.; Lorenzi, R.; Marchini, A.; Campone, L.; Sadeghi, E.; Paleari, A.; Sattin, S.; Gelain, F. Novel self-assembling cyclic peptides with reversible supramolecular nanostructures. *Materials Chemistry Frontiers* **2023**, *7*, 3680–3692.
- (41) Marrink, S. J.; Risselada, H. J.; Yefimov, S.; Tieleman, D. P.; De Vries, A. H. The MARTINI force field: coarse grained model for biomolecular simulations. *J. Phys. Chem. B* **2007**, *111*, 7812–7824.
- (42) Hammonds, K.; Heyes, D. Shadow Hamiltonian in classical NVE molecular dynamics simulations: A path to long time stability. *J. Chem. Phys.* **2020**, *152*.
- (43) Another reason may be the influence of Ref.<sup>93</sup>; however, note that such reference did not analyse explicit hydrogen atoms, hence its conclusions do not apply to H-angles.
- (44) Ortega, J. M.; Rheinboldt, W. C. *Iterative solution of nonlinear equations in several variables*; Computer science and applied mathematics; Academic Press: New York, 1970.
- (45) Kelley, C. T. *Iterative methods for linear and nonlinear equations*; Frontiers in applied mathematics 16; Society for Industrial and Applied Mathematics: Philadelphia, 1995.

- (46) Phillips, J. C.; Braun, R.; Wang, W.; Gumbart, J.; Tajkhorshid, E.; Villa, E.; Chipot, C.; Skeel, R. D.; Kalé, L.; Schulten, K. Scalable Molecular Dynamics with NAMD. *J. Comput. Chem.* **2005**, *26*, 1781–1802.
- (47) Phillips, J. C.; Hardy, D. J.; Maia, J. D.; Stone, J. E.; Ribeiro, J. V.; Bernardi, R. C.; Buch, R.; Fiorin, G.; Hénin, J.; Jiang, W.; others Scalable molecular dynamics on CPU and GPU architectures with NAMD. *J. Chem. Phys.* **2020**, *153*.
- (48) Pearlman, D. A.; Case, D. A.; Caldwell, J. W.; Ross, W. R.; Cheatham III, T. E.; DeBolt, S.; Ferguson, D.; Seibel, G.; Kollman, P. AMBER, a computer program for applying molecular mechanics, normal mode analysis, Molecular Dynamics and free energy calculations to elucidate the structures and energies of molecules. *Comp. Phys. Commun.* **1995**, *91*, 1–41.
- (49) Brooks, B. R. et al. CHARMM: The biomolecular simulation program. *J. Comput. Chem.* **2009**, *30*, 1545–1615.
- (50) Lou, G. Parallel methods for solving linear systems via overlapping decomposition. M.Sc. thesis, University of Illinois at Urbana-Champaign, 1989.
- (51) Golub, G. H., Van Loan, C. F., Eds. *Matrix Computations*, 2nd ed.; The Johns Hopkins University Press: Baltimore and London, 1993.
- (52) Karypis, G.; Kumar, V. Multilevelk-way partitioning scheme for irregular graphs. *Journal of Parallel and Distributed Computing* **1998**, *48*, 96–129.
- (53) Amestoy, P. R.; Davis, T. A.; Duff, I. S. An approximate minimum degree ordering algorithm. *SIAM Journal on Matrix Analysis and Applications* **1996**, *17*, 886–905.
- (54) Martin, C.; Richard, V.; Salem, M.; Hartley, R.; Mauguén, Y. Refinement and structural analysis of Barnase at 1.5 Å resolution. *Acta Crystallographica Section D: Biological Crystallography* **1999**, *55*, 386–398.

- (55) Mackerell Jr., A. D.; Feig, M.; Brooks III, C. L. Extending the treatment of backbone energetics in protein force fields: Limitations of gas-phase quantum mechanics in reproducing protein conformational distributions in molecular dynamics simulations. *Journal of Computational Chemistry* **2004**, *25*, 1400–1415.
- (56) Jorgensen, W. L.; Chandrasekhar, J.; Madura, J. D.; Impey, R. W.; Klein, M. L. Comparison of simple potential functions for simulating liquid water. *The Journal of Chemical Physics* **1983**, *79*, 926–935.
- (57) Cotton, F.; Hazen Jr., E.; Legg, M. Staphylococcal nuclease. Proposed mechanism of action based on structure of enzyme-thymidine 3',5'-biphosphate-calcium ion complex at 1.5-angstroms resolution. 1977; <https://www.rcsb.org/structure/2SNS>, RCSB Protein Data Bank entry, Accessed: 2023-09-27.
- (58) Douangamath, A.; Fearon, D.; Gehrtz, P.; Krojer, T.; Lukacik, P.; Owen, C. D.; Resnick, E.; Strain-Damerell, C.; Aimon, A.; others Crystallographic and electrophilic fragment screening of the SARS-CoV-2 main protease. *Nat. Comm.* **2020**, *11*, 1–11.
- (59) Núñez-Rojas, E.; Flores-Ruiz, H. M.; Alejandre, J. Molecular dynamics simulations to separate benzene from hydrocarbons using polar and ionic liquid solvents. *Journal of Molecular Liquids* **2018**, *249*, 591–599.
- (60) Schmid, N.; Eichenberger, A. P.; Choutko, A.; Riniker, S.; Winger, M.; Mark, A. E.; van Gunsteren, W. F. Definition and testing of the GROMOS force-field versions 54A7 and 54B7. *European Biophysics Journal* **2011**, *40*, 843–856.
- (61) Wu, B.; Mohideen, K.; Vasudevan, D.; Davey, C. A. Structural Insight into the Sequence Dependence of Nucleosome Positioning. *Structure* **2010**, *18*, 528–536.
- (62) Tian, C.; Kasavajhala, K.; Belfon, K. A. A.; Raguetta, L.; Huang, H.; Migués, A. N.; Bickel, J.; Wang, Y.; Pincay, J.; Wu, Q.; Simmerling, C. ff19SB: Amino-Acid-Specific

- Protein Backbone Parameters Trained against Quantum Mechanics Energy Surfaces in Solution. *Journal of Chemical Theory and Computation* **2020**, *16*, 528–552.
- (63) Zgarbová, M.; Šponer, J.; Jurečka, P. Z-DNA as a Touchstone for Additive Empirical Force Fields and a Refinement of the Alpha/Gamma DNA Torsions for AMBER. *Journal of Chemical Theory and Computation* **2021**, *17*, 6292–6301.
- (64) Izadi, S.; Anandakrishnan, R.; Onufriev, A. V. Building Water Models: A Different Approach. *The Journal of Physical Chemistry Letters* **2014**, *5*, 3863–3871.
- (65) Sui, H.; Han, B.-G.; Lee, J. K.; Walian, P.; Jap, B. K. Structural basis of water-specific transport through the AQP1 water channel. *Nature* **2001**, *414*, 872–878.
- (66) Huang, J.; Rauscher, S.; Nawrocki, G.; Ran, T.; Feig, M.; de Groot, B. L.; Grubmüller, H.; MacKerell, A. D. J. CHARMM36m: an improved force field for folded and intrinsically disordered proteins. *Nature Methods* **2017**, *14*, 71–73.
- (67) Huang, J.; MacKerell Jr, A. D. CHARMM36 all-atom additive protein force field: Validation based on comparison to NMR data. *Journal of Computational Chemistry* **2013**, *34*, 2135–2145.
- (68) Kim, J.; Oh, J. H.; Kim, D. Recent advances in single-benzene-based fluorophores: Physicochemical properties and applications. *Organic & Biomolecular Chemistry* **2021**, *19*, 933–946.
- (69) Levental, I.; Lyman, E. Regulation of membrane protein structure and function by their lipid nano-environment. *Nature Reviews Molecular Cell Biology* **2023**, *24*, 107–122.
- (70) Jo, S.; Kim, T.; Iyer, V. G.; Im, W. CHARMM-GUI: A web-based graphical user interface for CHARMM. *J. Comput. Chem.* **2008**, *29*, 1859–1865.
- (71) Lee, J. et al. CHARMM-GUI Input Generator for NAMD, GROMACS, AMBER,

- OpenMM, and CHARMM/OpenMM Simulations Using the CHARMM36 Additive Force Field. *Biophysical Journal* **2015**, *12*, 405–413.
- (72) Wu, E. L.; Cheng, X.; Jo, S.; Rui, H.; Song, K. C.; Dávila-Contreras, E. M.; Qi, Y.; Lee, J.; Monje-Galvan, V.; Venable, R. M.; Klauda, J. B.; Im, W. CHARMM-GUI *Membrane Builder* toward realistic biological membrane simulations. *J. Comput. Chem.* **2014**, *35*, 1997–2004.
- (73) Jo, S.; Kim, T.; Im, W. Automated builder and database of protein/membrane complexes for molecular dynamics simulations. *PLoS ONE* **2007**, *2*, e880.
- (74) Jorgensen, W. L.; Chandrasekhar, J.; Madura, J. D.; Impey, R. W.; Klein, M. L. Comparison of simple potential functions for simulating liquid water. *J. Chem. Phys.* **1983**, *79*, 926–935.
- (75) Izadi, S.; Anandakrishnan, R.; Onufriev, A. V. Building water models: a different approach. *J. Phys. Chem. Lett.* **2014**, *5*, 3863–3871.
- (76) Páll, S.; Hess, B. A flexible algorithm for calculating pair interactions on SIMD architectures. *Comput. Phys. Comm.* **2013**, *184*, 2641–2650.
- (77) Essmann, U.; Perera, L.; Berkowitz, M. L.; Darden, T.; Lee, H.; Pedersen, L. G. A smooth particle mesh Ewald method. *J. Chem. Phys.* **1995**, *103*, 8577–8593.
- (78) Haug, E. J.; Arora, J. S.; Matsui, K. A steepest-descent method for optimization of mechanical systems. *Journal of Optimization Theory and Applications* **1976**, *19*, 401–424.
- (79) Bussi, G.; Zykova-Timan, T.; Parrinello, M. Isothermal-isobaric Molecular Dynamics using stochastic velocity rescaling. *J. Chem. Phys.* **2009**, *130*, 074101.
- (80) Berendsen, H. J. C.; Postma, J. P. M.; van Gunsteren, W. F.; DiNola, A.; Haak, J. R.

- Molecular dynamics with coupling to an external bath. *J. Chem. Phys.* **1984**, *81*, 3684–3690.
- (81) Parrinello, M.; Rahman, A. Polymorphic transitions in single crystals: A new molecular dynamics method. *J. Appl. Phys.* **1981**, *52*, 7182–7190.
- (82) Galano-Frutos, J. J.; Sancho, J. Accurate Calculation of Barnase and SNase Folding Energetics Using Short Molecular Dynamics Simulations and an Atomistic Model of the Unfolded Ensemble: Evaluation of Force Fields and Water Models. *Journal of Chemical Information and Modeling* **2019**, *59*, 4350–4360.
- (83) Galano-Frutos, J. J.; Nerín-Fonz, F.; Sancho, J. Calculation of Protein Folding Thermodynamics Using Molecular Dynamics Simulations. *Journal of Chemical Information and Modeling* **2023**, *63*, 7791–7806.
- (84) Estrada, J.; Bernadó, P.; Blackledge, M.; Sancho, J. ProtSA: a web application for calculating sequence specific protein solvent accessibilities in the unfolded ensemble. *BMC Bioinformatics* **2009**, *10*, 104.
- (85) Bechtel, W. J.; Schellman, J. A. Protein stability curves. *Biopolymers* **1987**, *26*, 1859–1877.
- (86) García-Risueño, P.; Echenique, P.; Alonso, J. L. Exact and efficient calculation of Lagrange multipliers in constrained biological polymers: Proteins and nucleic acids as example cases. *J. Comput. Chem.* **2011**, *32*, 3039–3046.
- (87) García-Risueño, P.; Echenique, P. Linearly scaling direct method for accurately inverting sparse banded matrices. *J. Phys. A: Math. and Theor.* **2012**, *45*, 065204.
- (88) Mikkelsen, C. C. K.; Alastruey-Benedé, J.; Ibáñez Marín, P.; García-Risueño, P. Accelerating sparse arithmetic in the context of Newton’s method for small molecules

- with bond constraints. *Proceedings of the 11<sup>th</sup> International Conference on Parallel Processing and Applied Mathematics (PPAM)* **2016**, *I*, 160–171.
- (89) Kjelgaard Mikkelsen, C. C.; López-Villellas, L.; García-Risueño, P. How accurate does Newton have to be? *Proceedings of the 14<sup>th</sup> International Conference on Parallel Processing and Applied Mathematics (PPAM)* **2022**, *I*, 3–15.
- (90) Kjelgaard Mikkelsen, C. C.; López-Villellas, L. The need for accuracy and smoothness in numerical simulations. 2024.
- (91) Zlatev, Z.; Dimov, I.; Faragó, I.; Ágnes Havasi *Richardson Extrapolation: Practical Aspects and Applications*; De Gruyter, 2018.
- (92)  $k_B$  is Boltzmann constant;  $\hbar$  is the reduced Planck constant;  $T$  is the temperature.
- (93) Van Gunsteren, W. F.; Karplus, M. Effects of constraints on the dynamics of macromolecules. *Macromolecules* **1982**, *15*, 1528–1544.
- (94) Fábíán, B.; Thallmair, S.; Hummer, G. Optimal bond constraint topology for molecular dynamics simulations of cholesterol. *J. Chem. Theory and Comput.* **2023**, *19*, 1592–1601.